

CHALMERS



Modeling of Bonnet in LS-DYNA for Pedestrian Research

Master's thesis in Automotive Engineering

HAMIDREZA MAHMOUDI

Department of Applied Mechanics

Division of Vehicle Safety

CHALMERS UNIVERSITY OF TECHNOLOGY

Gothenburg, Sweden 2013

Master's thesis 2013:44

MASTER'S THESIS IN AUTOMOTIVE ENGINEERING

Modeling of Bonnet in LS-DYNA for Pedestrian Research

HAMIDREZA MAHMOUDI

Department of Applied Mechanics
Division of Vehicle Safety
CHALMERS UNIVERSITY OF TECHNOLOGY
Gothenburg, Sweden 2013

Modeling of Bonnet in LS-DYNA for Pedestrian Research
HAMIDREZA MAHMOUDI

© HAMIDREZA MAHMOUDI, 2013

Master's thesis 2013:44
ISSN 1652-8557
Department of Applied Mechanics
Division of Vehicle Safety
CHALMERS UNIVERSITY OF TECHNOLOGY
SE-412 96 Gothenburg
Sweden
Telephone: +46(0)31-772 1000

Cover:
An Articulate Expression of the Bonnet Modeling

Chalmers
Gothenburg, Sweden 2013

Modeling of Bonnet in LS-DYNA for Pedestrian Research
Master's thesis in Automotive Engineering
HAMIDREZA MAHMOUDI
Department of Applied Mechanics
Division of Vehicle Safety
Chalmers University of Technology

ABSTRACT

Pedestrians are the most vulnerable road users and crash statistics implies that continuous efforts are needed to reduce the causalities and mitigate their effects; both in passive and active safety. Current thesis is an attempt to provide a FE model which can be utilized for the analysis of the pedestrian kinematics. The author has focused on the bonnet modeling in LS-DYNA; furthermore, the modeling task was developed to provide the model of other influencing components in vehicle's front end namely: fenders, engine cover, battery cover and frame.

Through the use of GeoMagic studio, CATIA, HyperMesh, LS-Prepost and LS-DYNA, the FE models of all previously cited parts are prepared respectively. To investigate the response of the model to head and torso impacts, Euro-NCAP Head-form impacts tests were simulated and the responses evaluated. Also a FE model of a rigid torso impactor is modeled in LS-DYNA based on a mechanical torso impactor designed at Autoliv and the simulation results were compared and evaluated with the impact tests performed at Autoliv.

A first investigation deals with the response of the bonnet when exposed to different loads at different positions on the bonnet. It was found that the kinematics was influenced mainly by the stiffness of the collision point and particularly if the rigid parts were engaged in the impact and the size of the gap between the hood and the rigid components. A second study involves the comparison between the results of available experiments and those obtained in reconstruction of these experiments. Despite showing comparable peak acceleration and impact duration, the results indicated a significant discrepancy in terms of the shape and slope at the beginning of the impact. Finally, through the use of a parametric study, the effects of thickness, material, position tolerance, tolerance of velocity and impactor angle were investigated.

Key words: Bonnet FE modeling, Vehicle front FE modeling, Rigid torso impactor and impact tests, Euro NCAP headform impact tests, Parametric study, GeoMagic studio, CATIA, HyperMesh, LS-Prepost, LS-DYNA.

ACKNOWLEDGEMENTS

This thesis was carried out at Chalmers University of Technology and SAFER (Vehicle and Traffic Safety Centre at Chalmers).

I would especially like to show my appreciation for my examiner, Dr. Johan Davidsson, for providing the opportunity of working on this project and also for providing the necessary data for implementation of this project.

Special thanks are also given to the head of the division of vehicle safety, Dr. Karin Brolin, for her valuable discussions.

Several experts at Autoliv and SAFER have also provided data for the project and deserve to be acknowledged. They include technical specialist and group leader, Bengt Pipkorn of Autoliv, and design engineer, Christian Forsberg of Autoliv, for providing the mechanical properties of material and the test report of the rigid torso impact experiments for this work. I would also like to thank Dr. Jikuang Yang of Chalmers University of Technology for providing the FE head-form impactors for this project. And thanks to PhD students, Linus Wågström and Manuel Mendoza-Vazquez for their helpful consults.

Also, I want to thank the UK & Northern European Regional manager of Geomagic, Mr Steven Fletcher.

Finally, I am extremely grateful to my parents who have supplied me with unlimited support and encouragement throughout my years of study; and I would like to dedicate this thesis to my father and my mother who have tried to making me a better person.

Göteborg, 2013

Hamidreza Mahmoudi

NOMENCLATURE, DEFINITIONS AND ABBREVIATIONS

CATIA

Computer Aided Three-dimensional Interactive Application

E

Elasticity Modulus

FEA

Finite Element Analysis

GeoMagic Studio

Geomagic software products have focused on the process of 3D capture into usable 3D data so the models can be used in engineering, product design, art, archaeology, medical procedures and archival purposes.

HBMs

Human Body Models

HIC

Head Injury Criterion

HyperMesh

A pre-processing tool for model build-up. Includes CAD and meshing tools as well as material and property information used in LS-DYNA and other simulation software.

LS-DYNA

An advanced general-purpose multi physics simulation software package developed by the Livermore Software Technology Corporation (LSTC).

NCAP

New Car Assessment Programme

STL

Standard Tessellation Language or Stereo Lithography

ϵ_{ep}

Effective Plastic Strain

ϵ_{tt}

Total True Stress

σ_t

True Stress

CONTENTS

ABSTRACT	I
ACKNOWLEDGEMENTS	III
NOMENCLATURE	V
CONTENTS	VI
1 INTRODUCTION	1
1.1 Background	1
1.2 Objective	1
1.3 Scope	2
2 METHOD	4
2.1 Scanning of Renault Megane	5
2.2 Scan modification using Geomagic Studio	7
2.3 Surface reconstruction using CATIA	9
2.4 FE Mesh generation using HyperMesh	12
2.4.1 Mesh Size	12
2.4.2 Aspect ratio	13
2.4.3 Jacobian	13
2.4.4 Warpage	13
2.4.5 Skewness	13
2.5 Reconstruction of Euro-NCAP head impacts in FE model	14
2.6 Reconstruction of rigid torso impacts in FE model	15
2.7 Preparation of Cards in LS-DYNA	16
2.7.1 Material	16
2.7.2 Section	17
2.7.3 Boundary	17
2.7.4 Hourglass	18
2.7.5 Velocity	18
2.7.6 Impactor Positioning	18
2.7.7 Accelerometer for Rigid torso impactor	20

2.7.8	History node for rigid torso impact simulation	20
2.7.9	Miscellaneous	21
3	RESULTS	22
3.1	Preliminary Control	23
3.2	Adult HF Impactor CP01	24
3.2.1	Experiment vs. simulation	24
3.2.2	Velocity comparison	25
3.2.3	Impact angle comparison	25
3.3	Adult HF Impactor CP02	27
3.3.1	Experiment vs. simulation	27
3.3.2	Different Materials	27
3.4	Child HF Impactor CP10	28
3.4.1	Experiment vs. simulation	28
3.4.2	Thickness variation	29
3.5	Child HF Impactor CP09	30
3.5.1	Experiment vs. simulation	30
3.5.2	Stiffness contribution	30
3.5.3	Positioning	31
3.6	Child HF Impactor CP08	32
3.6.1	Experiment vs. simulation	32
3.6.2	Positioning comparison	32
3.7	Child HF Impactor CP07	33
3.7.1	Experiment vs. simulation	33
3.7.2	Stiffness contribution	33
3.8	Rigid Torso Impactor	34
3.8.1	Front edge alignment	34
3.8.2	Rear edge alignment	34
4	DISCUSSION	36
5	CONCLUSION	39
6	REFERENCES	41
7	APPENDICES	42
7.1	Scans characteristics	43
7.2	CAD and scan comparison	44
7.3	Mesh	45
7.3.1	Meshed models	45

7.3.2	Mesh quality report	46
7.4	Head impact tests no. CP0242xx; Euro-NCAP	47
7.4.1	Visual inspection after tests	47
7.4.2	Velocity, angle and mass	48
7.4.3	Impact position	48
7.4.4	Head Injury Criterion	48
7.5	Rigid torso impact tests; Autoliv.	49
7.5.1	Test L212009	49
7.5.2	Test L212010	50

1 Introduction

This study includes several steps of mathematical model creation for the front part of a factory-made vehicle, starting with scanning the vehicle geometry resulted in form of points cloud, being developed by surface reconstruction in CATIA for the aforementioned points cloud and ending in a FEM-based or LS-DYNA model useful for simulations of pedestrian crashes. In addition, an evaluation was carried out; here the aim was to study the acceleration of both head-form and torso impactor, the causes of deviation between experiment and simulation data as obtained in the evaluation study were investigated using various parametric studies.

1.1 Background

Pedestrians are the most vulnerable human beings in collisions since they are not protected as those that are restrained inside the vehicles' compartment. Sixty-five percent of accidents worldwide involve pedestrians; the pedestrian's head suffers from the most frequent and serious injuries followed by lower limb and upper limb injuries in terms of severity and numbers, respectively.[10]. In order to reduce these injuries both active and passive safety require additional attention. For passive safety there is a need for improved test tools; both readily available mechanical dummies and improved mathematical models of the human (HBMs) are needed. For the latter there is need for pertinent evaluation data. Commonly such data is generated in the laboratory; post

mortem human subjects (PMHS) are impacted by a vehicle. This thesis is on the development of a Finite Element (FE) model of a car that was used in PMHS tests; such a model will facilitate a reconstruction of the PMHS tests using various pedestrian HBMs. The focus is on the development of a model of the bonnet.

The role of bonnet in head impact has been given a great prominence; according to a study by Peng et al on child pedestrian impact, the head impact point is located on the bonnet in all types of vehicles included in their study. These were small Super Mini Car (SMC), Small Family Car (SFC), large Family Car (LFC), Multi-Purpose Vehicle (MPV), and Sport Utility Vehicle (SUV). For an adult pedestrian, the impact point is located on the bonnet for SUV and LFC and in the other cases the impact point is located on the windshield. Although, in 3 cases out of 5 types of vehicle, the head collided to the windshield based on their results, but the recent developments and design of active mechanisms for lifting the bonnet edge has lowered and even removed the risk and probability of head impact to the windshield.[9].

In addition, it has been suggested that the thorax and elbow to bonnet contact highly influence the head kinematics and as such the risk of head injury in case of contact with the vehicle.

1.2 Objective

There is an increasing demand for the development of FE HBMs for simulation of

pedestrian crashes. However, evaluation of such models requires PMHS data and reliable vehicle models. Thus, this thesis focus on the modeling of the bonnet in particular, and the relevant structures like fenders and engine housing's components influencing the behavior of the bonnet in pedestrian crash simulations which may lead to increase or decrease of injury severity.

1.3 Scope

In order to establish an HBM evaluation environment, the preliminary scope of this thesis is to provide FE-model of the bonnet. Afterwards, it is developed to creation of model for other components in the front part of the car used in PMHS tests in the past.

To investigate the effect of bonnet and the vehicle front on pedestrians kinematics in impact, 3 different structures are modeled based on the scan of the vehicle; simplified, intermediate and sophisticated structure were simulated in LS-DYNA and evaluated. The complexity of the models was defined as the contribution of components in impact. In the simplified case, the outer panel of the bonnet is modeled and in the intermediate case, the outer panel and inner panel are modeled. Finally in the sophisticated case, the entire vehicle front including the bonnet's inner panel, bonnet's outer panel, fenders, engine cover, battery cover and the frame under the bonnet are modeled and simulated.

Two limitations in this thesis concern the modeling of the hinges and the latch; the degrees of freedom of the hinges and the latch of the bonnet were assumed as zero. This was considered acceptable as the existing height

regulators situated underneath the bonnet were very stable and in close contact with the bonnet.

For evaluation of the FE models, Euro NCAP head-form impacts to the bonnet have been reconstructed. Additionally, a simplified FE model of a rigid semi box-shape impactor that represents the torso of a pedestrian is modeled, developed and used in reconstructions of torso-to-bonnet tests conducted by Autoliv.

2 Method

- 2.1 Scanning of Renault Megane
- 2.2 Scan modification using GeoMagic Studio
- 2.3 Surface reconstruction using CATIA
- 2.4 FE mesh generation using HyperMesh
- 2.5 Reconstruction of the NCAP head impacts
- 2.6 Reconstruction of the torso impacts
- 2.7 Preparation of cards in LS-DYNA

2.1 Scanning of Renault Megane

CAD models of the components to be used in LS-DYNA were not available. Hence, these were scanned (Cascade, Sweden) using an ATOS with the accuracy of 15 micro meters to 0.789 mm; this was considered sufficient for the goal of this project.

In the scanning process, Vehicle's front end was scanned including the bumper, the fenders, top view of engine housing, the bonnet outer and inner panels. The whole front end was scanned while the bonnet was in normal position and closed; afterwards, the engine housing' parts were scanned, In the latter stage the upper edge of the fenders were scanned for assembling in the right position with respect to the scanned components' position in the first stage. And finally, the inner skin of the bonnet was scanned.

The global coordinate's origin has been located in the intersection of the three planes representing the ground surface, longitudinal symmetry plane of the vehicle and a tangential plane of the bumper tip which is

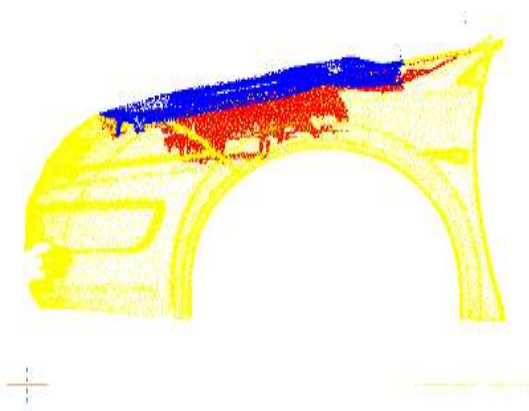


Figure 2.1.1 - Scanned model, left view

also perpendicular to the ground. Figure 2.1.1 and figure 2.1.2.

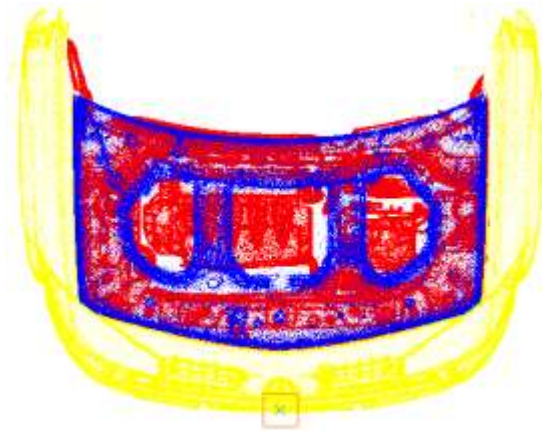


Figure 2.1.2- Scanned model, top view

The scanner exported STL format data (Standard Tessellation Language or Stereo Lithography) which is usable in computer-aided manufacturing (CAM). Basically, the STL model consists of raw triangulated facets, see figure 2.1.3, in which the vertex is selected from a cloud of points so that every three points which are in the vicinity of each other generate a facet subsequently, and consequently, the combination of all those facets make up the scanned model.

One disadvantage with the STL format was that files of this format could not be used in further stages of the project for generating mesh since it is not a mathematical representation of the geometry and it did not contain the CAD attributes. Therefore, another format for instance IGES should be used instead of STL, containing the data for Non-uniform rational basis spline (NURBS) curve and NURBS surface which are commonly used in computer-aided design (CAD) and engineering (CAE).

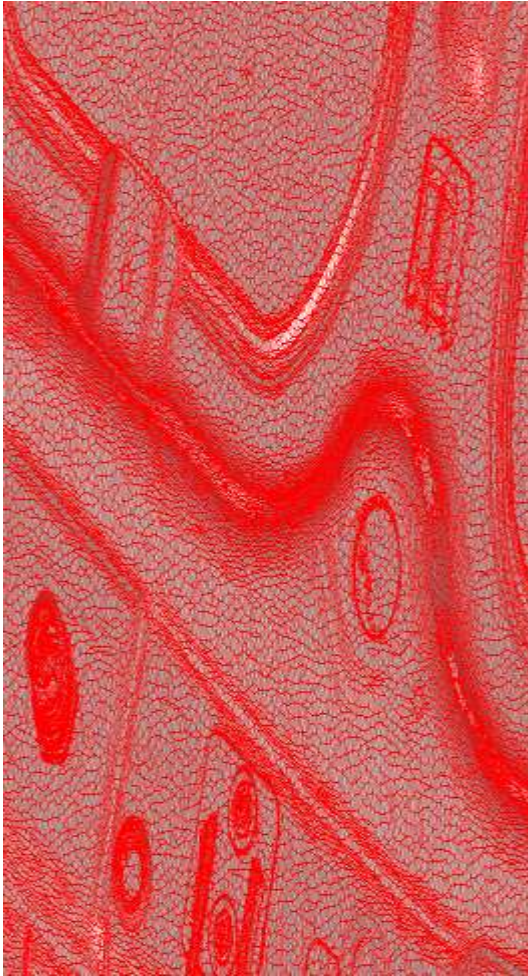


Figure 2.1.3 - Triangulated model

NURBS is a mathematical model commonly used in computer graphics for generating and representing curves and surfaces.

GOM Inspect which is the software linked to the scanner was able to export the IGES format of the curves extracted from intersection of any arbitrary plane with the scanned model; but it was only (IGES section) and the software cannot export the surface and solid in IGES format directly from scan. GOM Inspect provides some

surface reconstruction features for basic elements like cylinder, cone and etc., while the model contains complicated elements; so it was identified that interface software was needed for surface generation of such a sophisticated model.

Despite having few features for reconstructing surfaces, GOM Inspect is a great tool for inspection and quality purposes, a tool with the capability of measuring the dimensional deviations between physical models and CAD models, Moreover it provides the inspectors special options to check the geometrical tolerances using GD&T section in the software.

In a distinct section, surface reconstruction using CATIA will be explained, but should be mentioned that the scanner was not able to capture the 3D image of the model completely due to the lack of accessibility to those regions; because of this matter, the scan needs to be modified in some area and the process of modification is explained in the next section.

2.2 Scan modification using Geomagic Studio

As explained in the previous section, the scan of the physical model was found not perfect in some regions, and some filling was required; beside these issues, there are parts which are not important like rubbery hosing underneath the bonnet which has no influence on the stiffness of the bonnet and it merely increases required time and complexity in the process of surface reconstruction.

In addition to the issues cited above, there are some other modifications implemented in scan which will be explained later in this section.

In order to implement the desirable corrections in the scan, Geomagic Studio was selected which provided user friendly and time-effective features.

Compared with CATIA, Geomagic studio is faster and the generated mesh is smoother and more consistent with the elements in its vicinity, meaning that the deviation between the generated mesh and target model decreases.

First, each part was separated from the entire assembly by deleting the irrelevant components and was saved in a distinct file. And the mesh clean-up was been done part by part.

Below, the pictures showing the scan's faults in the bonnet's panels imply how time consuming was the process of mesh clean-up and where the modifications have been carried out by means of Geomagic Studio.

In this section, the modification and its detailed explanation have been concentrated

on the bonnet, trying to present the modified zones in various detail views.

The red polylines in the figures represent the original edges around the holes, notches and outermost boundaries of the components which exist in the physical model, Also they represent undesirable edges around the holes generated due to the lack of data from scanning process.

For instance, detail views A and B show several holes, small and big, where the scanner could not obtain the data in those areas due to the dimensions of the scanner and the difficulty in disassembling the bonnet. All similar types of closed holes like what has been magnified in detail views A and B, were selected and filled up using the intelligent features provided in Geomagic.

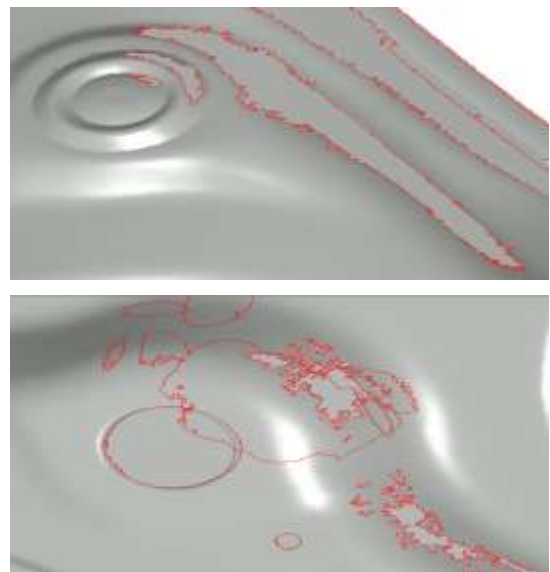


Figure 2.2.1-Detail views: A (up) and B (down)

In the areas illustrated in detail views C and D, the hosing was erased due to its stiffness contribution considered negligible since the material is rubber and very flexible. Afterwards, the remaining holes were treated

as explained in previous paragraph. in the process of filling up holes, a priority was considered to avoid a significant change in the topology of the model in that specified area; some trials and errors were done and the results showed that starting with small holes concludes in the least changes in neighboring elements and the resultant shape became more consistent within the specific zone of

A similar measure was taken and the hinges in both sides were deleted including the bolts. Meanwhile, there were some small holes in the bonnet-physical model- that could not influence on the result significantly, so they were eliminated too for generating more aligned and organized mesh in the next steps. See figure 2.2.4, detail views F and G.

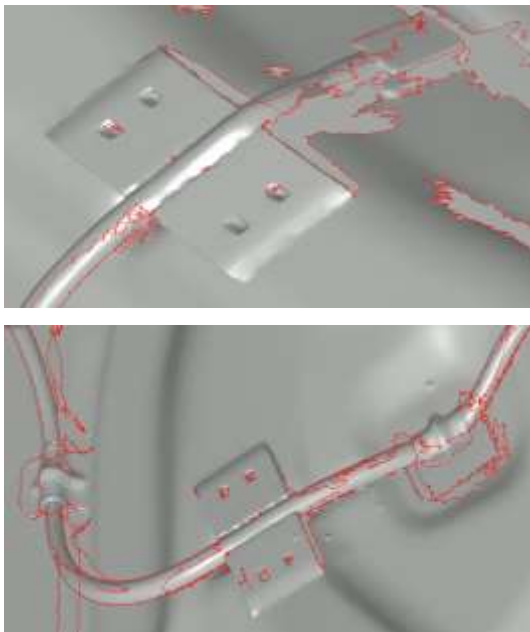


Figure 2.2.2- Detail views: C (up) and D (down)

modification and outside.

The U-shaped rod which is a part of the bonnet latch and the spring in its vicinity, were deleted to simplify the model for surface reconstruction. See figure 2.2.3, detail view E.

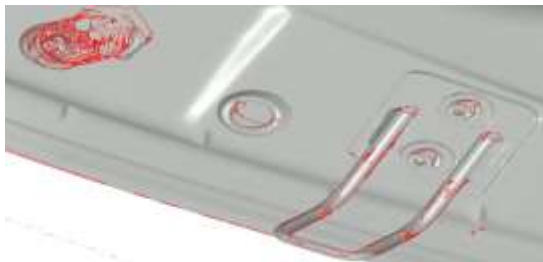


Figure 2.2.3- Detail view: E

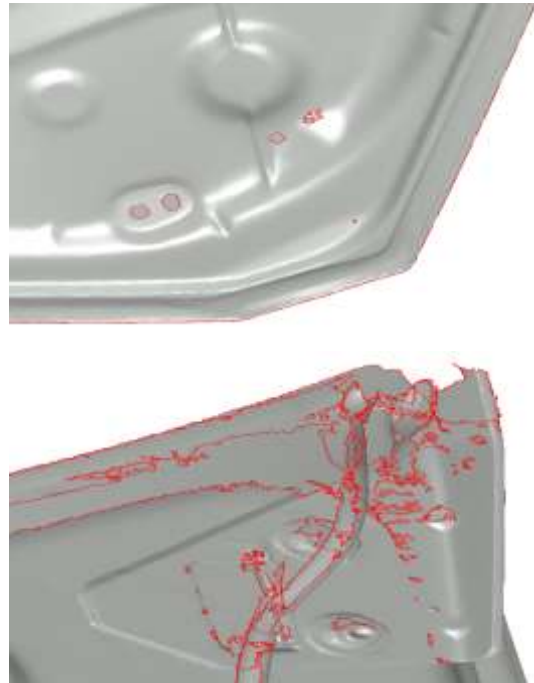


Figure 2.2.4- Detail views: F (up) and G (down)

2.3 Surface reconstruction using CATIA

After preliminary clean-up and mesh generation by means of Geomagic Studio in the areas depicted in the previous section, relatively modified mesh is imported into CATIA in a module called digitized shape editor for final stage of clean-up. This module provided a powerful tool for detecting any sort of defects in the model including duplicated triangle, corrupted triangle, non-manifold edges, non-manifold vertices and isolated triangles so that they could be deleted or modified easily.

Below are some examples and definitions of the aforementioned defects and irregularities illustrated in figure 2.3.1, [1]:

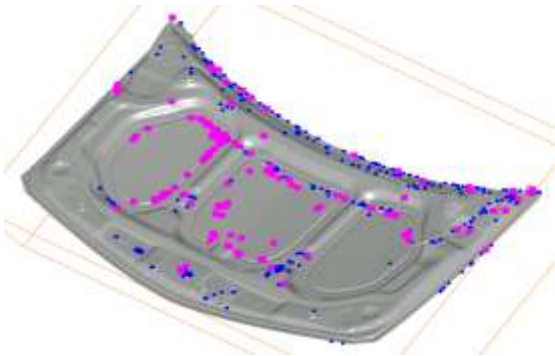


Figure 2.3.1- Sporadic irregularities in Scan

- *Corrupted triangles, i.e. triangles that have the same vertex twice, red, Figure 2.3.2*
- *Duplicated triangles, i.e. triangles that share the same three vertices, cyan, Figure 2.3.2*
- *Inconsistent orientation, i.e. triangles that cannot be oriented consistently with respect to each other, yellow, Figure 2.3.2*
- *Non-manifold edges, i.e. edges shared*

by more than two triangles, magenta Figure 2.3.2

- *Non-manifold vertices, i.e. vertices shared by two or more connected shells. Blue Figure 2.3.2*

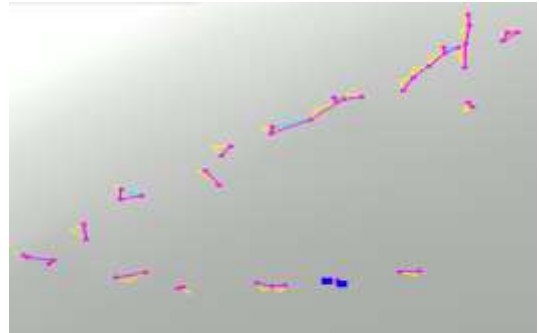


Figure 2.3.2- Irregularities in detail view

A mesh may also present some structural problem such as, [1]:

- *Orientation problems, i.e. all the triangles are not in the same direction,*
- *Isolated triangles, i.e. triangles belonging to small connected areas of the mesh,*
- *Disconnected zones, i.e. the mesh is made of several disconnected zones, Figure 2.3.3*
- *Triangles with long edges,*
- *Thin triangles.*

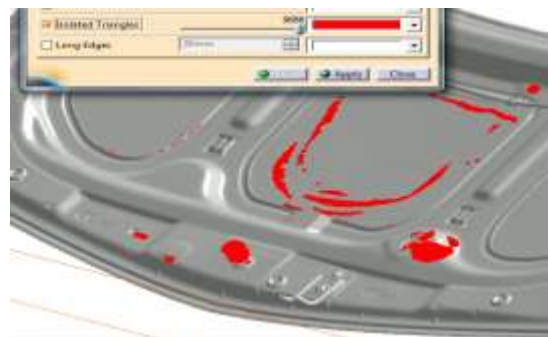


Figure 2.3.3-- Isolated triangles and disconnected zones

In addition to mesh cleaner feature, there were some other useful features which have been utilized during the process of mesh clean-up. For instance, feature ' Interactive Triangle Creation' was used to modify and align the edges in some areas.

Some other features were not used like 'Optimise' and 'Mesh Smoothing', because they could change the geometrical attributes of the model.

Generally speaking, the detection of mesh defects , clean-up and generation have been carried out in An iteration cycle by means of Digitized Shape Editor module of CATIA and Geomagic Studio software to remove all problematic elements and to replace suitable elements subsequently.

At the point when the mesh modification was completed, the model was prepared to be exported to another module of CATIA called Quick Surface Reconstruction. Depending on the complexity of the models shape, this module provided relevant feature for reconstructing the surfaces.

In the beginning of the surface reconstruction process, the basic surfaces and elements were recognized visually, namely simple planes, lines, polylines, circles, cones etc. Afterwards those elements were generated using available features in the module. Further down a detailed explanation of those jobs will be illustrated by means of several relevant figures.

Mesh orientation, mesh and the elements configuration is important; these should be

developed so that their sides - Quad Elements specifically - are placed parallel to each other. And this is quite dependent to the orientation of the surface patch's sides. The stiffness of the model will increase if the quads are non-parallel significantly.

The procedure of surface reconstruction is explained briefly for the outer panel of the bonnet in a few steps below. As can be seen in the figure (14), the planar sections are created from the intersection of a certain plane with the bonnet scan in any arbitrary direction. For instance, this process is illustrated in figure 2.3.4 in which the nine planar sections have been generated through the use of relevant feature in CATIA. It should be noted that the purpose is to define the boundaries of the zone of interest for surface reconstruction. Wherever those boundaries represent the form of the scan, an appropriate surface with the shape of scan can be expected and reconstructed.

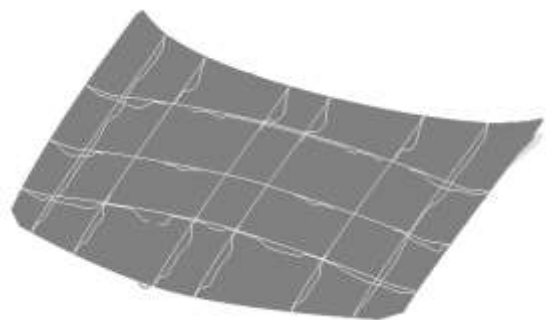


Figure 2.3.4- Planar sections

Afterwards, the group of the curves generated at the arbitrary sections can be

made as partially depicted in figure 2.3.7 for the outer panel of the bonnet. It is evident that the shape of the bonnet was adequately presented by the network curve and this was proved by having a closer look at the curvature of the splines being placed in the longitudinal and lateral directions of the bonnet. Essentially, to have a perfect network curve in the region of interest, the connection of the splines with each other should be checked and ensured to make the surface reconstruction possible in the next stage, meaning that the neighboring curvilinear rectangles should have common vertices.

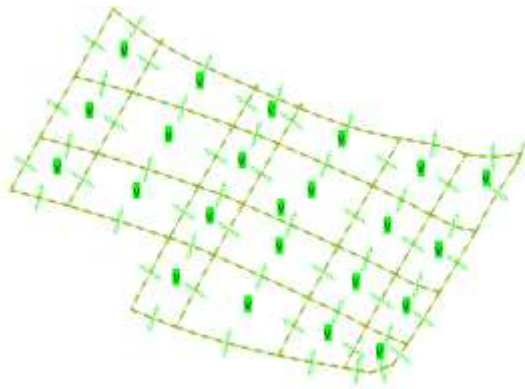


Figure 2.3.5 - Network curve creation

Figure 2.3.5 shows some of the surfaces reconstructed using the generated network curve and scan data. Whatever briefly explained so far is one of the methods used for reconstructing the surfaces, whilst there are other alternatives which have not been explained to avoid repetition and monotony.

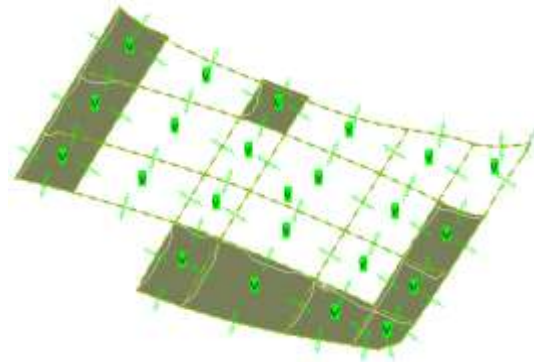


Figure 2.3.6- Surface reconstruction using generated network curve

Finally, a comparison was carried out between the reconstructed surface for the bonnet and the target scan. And the result was evaluated using deviation analysis feature provided in CATIA. It is obvious that the deviation is around half a millimeter or even less for the most part and the maximum deviation appeared at the edges will not substantially influence the geometry of the main body of the bonnet. The CAD models and the relevant deviation analysis of the other parts are available in the appendix section.

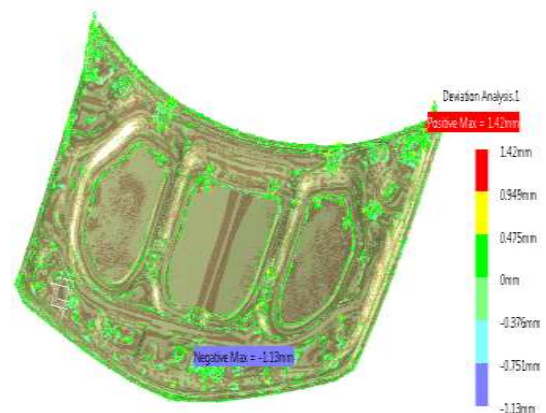


Figure 2.3.7- Deviation analysis between scan and reconstructed surface

2.4 FE Mesh generation using HyperMesh

Initially, the imported model as IGES, was controlled for the corrupted and twisted surfaces and also for the boundaries and edges between surfaces where the gap in between is beyond the acceptable range. See figure 2.4.1.

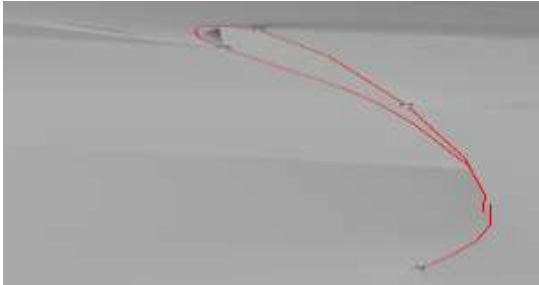


Figure 2.4.1- Gap among surfaces in imported IGES

The modifications are followed by suppressing the boundary patches to avoid the undesirable layout of the mesh which was explained earlier. See figure 2.4.2.

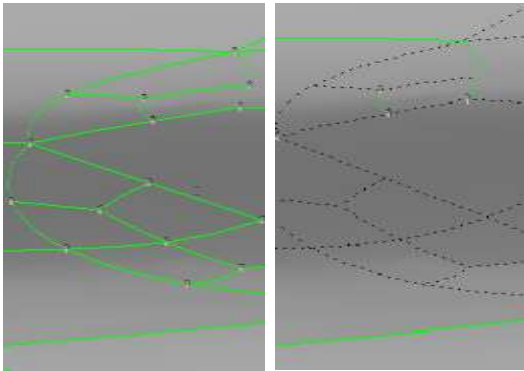


Figure 2.4.2– Suppression of patches' boundaries before (left) and after (right) implementation

Now the criteria for a suitable mesh type, size and geometrical attributes will be described. There are two different 2D mesh types, namely quads and trias. The quads show better results in comparison with trias, nevertheless degenerate quads are not

preferred as compared to trias with acceptable quality. Additionally, the degenerate quads are those which their vertices' angle is far less or far more than 90 degrees. Meanwhile the resultant values using both types are approximate and not an exact solution. Hence, each model's surfaces were meshed using Automatic 2D Mesh with a combination of trias and quads. However, the resulting mesh comprised mainly of quad elements.

2.4.1 Mesh Size

Basic dynamics of a system can be investigated using a coarse mesh, but a finer mesh is required to show the nonlinear behavior of the material and failure.

In the meshing application, the aim was to keep the majority of the elements size around 4 mm which is finer/smaller than the mesh size-around 10 mm in the bonnet- applied in NCAC models; The size of the mesh was determined based on the size of the free motion head-form impactor which was supposed to be used in early stages of the project. Moreover, the finer/smaller meshes are able to adapt to the topology and the underlying mathematical definition of the CAD model. Using this approach, the smaller elements are less likely to be distorted when the structure is subjected to large deformations. But on the other hand, applying finer mesh raises the simulation time duration due to the explicit nature of the solver for dynamic analysis.

Aside from the size of the mesh, there are some other criteria which are important and mesh should be checked based on the acceptable values defined for those criteria,

namely: aspect ratio, warpage, skewness, Jacobian, minimum and maximum vertices angle in quads and trias.

Following text reviews a brief explanation of the aforementioned criteria:

2.4.2 Aspect ratio

It shows the ratio of the longest side to the shortest side of an element and it should be less than 5. See figure 2.4.3.

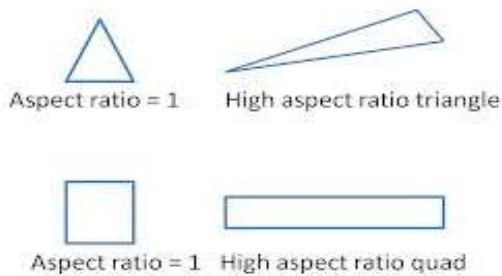


Figure 2.4.3– Aspect ratio schematic

2.4.3 Jacobian

A value represents the deviation of the element from the ideal shape is called Jacobian, varying between 0 and 1. The best value is one which represents a perfect element and the minimum acceptable value is 0.6.

2.4.4 Warpage

This defect appears in quad elements in which the 4 nodes of a quad element are not placed in a plane. The warpage angle is calculated based on the angle between the trias elements which can be generated after splitting the warped quad element.

The default setting of LS-DYNA accepts the warpage angle up to 20 degrees. The stringent acceptable range varies within the range of 0

to 7 degree, but the meshes applied to the bonnet, were optimized and kept under the warpage angle of 15 degree due to the large numbers of elements. And in the shell control card of LS-DYNA, the type of shell for warped element was overridden by the shell type No 10 which considers the warpage in the element formulation and computation.

2.4.5 Skewness

Skew angle that should be less than 60 degree, is 90 degree subtracted by the minimum angle between the lines connecting the opposite midpoints of the elements' sides in quads.

In trias the skewness is defined as the minimum angle between the lines connecting the nodes to the midpoint of the relevant opposite side and the line connecting the midpoints of that specific side of the node. See figure 2.4.4.

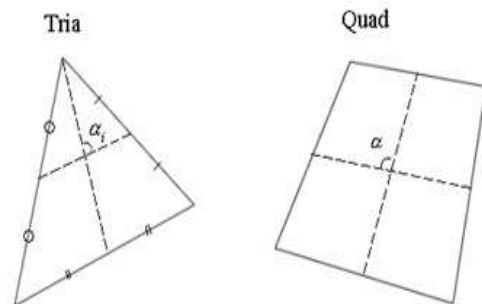


Figure 2.4.4– Skew angle schematic

Considering the aforementioned criteria and after application of the acceptable range defined in HyperMesh, the meshed model is prepared. The meshed model and the mesh quality report are available in the appendices.

2.5 Reconstruction of Euro-NCAP head impacts in FE model

In this section, the essential data and specification of Euro-NCAP head impact tests are collected to be used for preprocessing of models in LS-DYNA. The Euro NCAP pedestrian protection impact tests on a Renault Megane were conducted in October 2002 and reported as TNO tests no.: CP024205-CP024306. The experiments were carried out at the Crash Safety Centre in Delft, Netherlands.

Through the use of aforementioned report, the essential data regarding the head form impact are collected to be utilized in the simulation of the impacts in LS-DYNA in order to evaluate the performance of the bonnet and vehicle front which will be modeled, and also to study the stiffness behavior of different impact points and the effects on the acceleration of impactor.

The test specifications are accordant with the Euro NCAP test protocol for pedestrian protection. Two types of head form impactors were used in the impact tests namely: adult and child; similarly, two FE head form impactors are selected with identical shape and mass. According to their manual, the calibrated models show 20% uncertainty in the resultant acceleration values of FE models.

The triaxial accelerometer of the mechanical impactor has recorded the acceleration values of head form impactor for 3 axes defined for the accelerometer of the impactor. Using those X, Y and Z acceleration values and the

following formula, the resultant acceleration is obtained as:

$$a_R = \sqrt{a_x^2 + a_y^2 + a_z^2} - a_c \quad (2.5.1)$$

As can be seen, a correction value termed a_c has been subtracted from the resultant acceleration; the experiments data show non-zero acceleration before and after impact and the aforementioned term is shifting the acceleration curve downward, making a new acceleration curve starting from zero at the initial moment of impact. The value was between 6g and 10g for different impact locations. This corrected value is used in the comparison figures of the results section.

In the test report, the velocity of impact was tabulated as $11.1 \pm 0.2 \left[\frac{m}{s} \right]$, thus the velocity of FE impactor in all simulations is considered as the target velocity for both adult and child headform impactors. Also, a comparison study is carried out for the velocity variation with the tolerance limits.

The impact angles of 65° and 50° are defined in the simulation for adult and child impactors as the values specified in the test report and Euro NCAP protocol for pedestrian protection.

Six out of ten impact locations are selected from those specified in the test report; these 6 impacts took place on the bonnet. The FE impactors are manipulated to the coordinates specified in the test report. The origin of the coordinates system of the FE headform impactor is modified based on the origin of the coordinates system of the mechanical head form impactor in Euro NCAP test.

The Euro NCAP impact test specifications are available in the appendix 7.4.

2.6 Reconstruction of rigid torso impacts in FE model

Based on a mechanical torso impactor designed at Autoliv, a simplified version of the mechanical impactor is modeled in LS-DYNA as following:

A finer mesh around 4 mm is regenerated for the semi box-shaped impactor after remodeling the impactor in CATIA based on provided dimensions.

The total mass of the impactor and the sliding structure connected to the impactor are modeled as a homogeneous mass in the FE model. According to the test report of the rigid torso impacts, the total mass is 12 kg and this is defined as density in the material card of the FE model; the density is computed using the mass and the volume of the FE model.

Since the mechanical impactor has been considered rigid in their design, and no deflection has been observed and reported, so the material of the FE impactor is modeled by MAT_RIGID (020) and the elasticity modulus is defined equal to the elasticity modulus of the bonnet to provide stability for the contact.

The accelerometer of the mechanical impactor was mounted in the middle of the impactor. The geometry of the FE model does not provide any node in the corresponding position; in order to mount a triaxial accelerometer in the FE impactor, a rigid beam is attached to the model and merged at the connecting nodes to follow the motion of

the impactor rigidly. And the accelerometer is mounted at the middle of the rigid beam.

Two impact tests have been conducted using the mechanical impactor and two spare bonnet of Renault Megane. The impact positions are different in these two impact tests; similarly, the tests are simulated in LS-DYNA for these two impact positions. In the first experiment, the FE impactor is aligned with the rear edge of the bonnet and in the second test, the FE impactor is aligned with the front edge of the bonnet and in an offset of 125 mm to the right.

According to the impact test report, the bonnet has fixed in 5 region of the inner skin with different degrees of freedom. In the front part, the bonnet was screwed, so all degrees of freedom at the corresponding region in the bonnet is removed. The physical bonnet has been placed on 4 plates with different areas, having 5 degrees of freedom at the aforementioned areas. Therefore, the FE bonnet is constrained in the vertical direction through a number of nodes at the corresponding regions.

The initial velocity of the FE impactor is defined as the reported impact velocity of mechanical impactor ($6.1 \frac{m}{s}$).

Two stringpots were installed under the bonnet to measure the deformation of the bonnet at two specific points, so the corresponding nodes in the FE bonnet are tracked using history node card in LS-DYNA.

The pictorial explanation of the impact tests conducted at Autoliv, are available at the appendices 7.5.1 and 7.5.2.

2.7 Preparation of Cards in LS-DYNA

After the mesh of the surfaces is generated, the model was prepared for simulation as explained below:

2.7.1 Material

2.7.1.1 Material of bonnet and fenders

The mechanical properties applied for the Bonnet's outer, inner skins and fenders were selected from a datasheet provided by Autoliv. See figure 2.7.1.

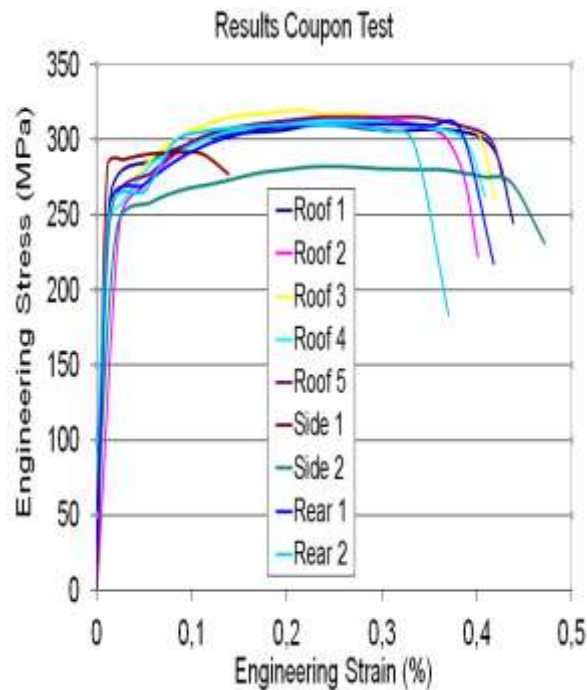


Figure 2.7.1– Stress vs. strain, provided by Bengt Pipkorn, Autoliv.

Since the input data in material card is effective plastic strain, the relevant values were obtained using experimental data and the following equation:

$$\varepsilon_{ep} = \varepsilon_{tt} - \sigma_t/E \quad (2.7.1)$$

(ε_{ep} = Effective plastic strain, ε_{tt} = total true strain, σ_t = true stress, E = Elasticity Modulus)

Therefore this means that the effective plastic strain modeled is the residual part of the strain which remains after unloading the elastic strain generated due to the specific true stress.

The extracted data has been depicted below. Piecewise Linear Plasticity was selected and utilized to model the mechanical properties of the bonnet including both outer and inner skins in LS-DYNA.

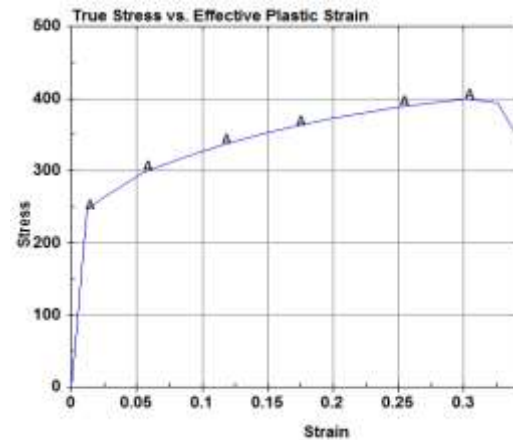


Figure 2.7.2- True stress vs. Effective plastic strain

2.7.1.2 Material of engine housing's components

The material of the engine housing's components including engine cover, battery cover and frame were assumed rigid; and the materials were assigned to the aforementioned parts using MAT_RIGID (020). The elasticity modulus and density were defined based on the values used for the bonnet and fenders to provide a stable contact between master and slave parts.

2.7.2 Section

Whereas the model has been prepared as a surface model, the shell element form was selected for the entire model and in this case, the element form is the default element form in LS-DYNA called Belytschko-Tsay which is mostly advised to be used for shell elements.

Another important thing that should be mentioned here is that one point was added to the number of through shell integration points and the NIP was set to 3.

2.7.2.1 Thickness of bonnet and fenders

The thickness of the bonnet sheet metal were measured by a caliper and recorded as 0.75 mm. This value was utilized in the section card as the thickness of the elements for the entire bonnet. Also, the thickness of shells in fenders were defined as much as the thickness of bonnet.

2.7.2.2 Thickness of engine housing's components and rigid torso impactor

The thickness of shells in engine housing's components and rigid torso impactor were defined 2 mm.

2.7.3 Boundary

2.7.3.1 Bonnet constraints in headform impact

To fix the bonnet in space, three SPC-Node sets were considered to model the fixed points of the bonnet in the areas where it is assembled on the plates of the hinges and also the area where the bonnet is constrained by the latch. Initially, a set of nodes were

selected for applying the boundary condition by means of SPC-Node set, representing the area of connection.

2.7.3.2 Bonnet constraints in rigid torso impact

Meanwhile, the bonnet was fixed with different setup for torso impact test. Figure 2.7.3 and figure 2.7.4 show how the bonnet was prepared for the experiment; in the front end of the bonnet where the latch had been assembled before the experiment; the bonnet was constrained by screwing a bolt after disassembling the latch. All 6 DOFs of the selected nodes in the FE model were constrained in the aforementioned SPC-Node set.

In addition to above, there were two devices to adjust the height of the bonnet in the front end when installed in the car. In the experiments, these adjustments were replaced by two bolts in the same size of the mushroom-shaped regulators. And in the simulation, the relevant nodes were fixed in translational direction of the Z-axis.

In the rear end of the bonnet, the rightmost and the leftmost area underneath the bonnet where the hinges are assembled to the bonnet,



Figure 2.7.3– Constraints setup for latch and regulators, provided by Christian Forsberg, Design Engineer, Autoliv.

a set of nodes has been selected in each side to be constrained in the Z direction.



Figure 2.7.4– Constraints setup for hinges, provided by Christian Forsberg, Design Engineer, Autoliv.

2.7.4 Hourglass

Four-node quadrilateral elements of the mesh in Explicit Dynamics are prone to show 'Hourglass' modes of deformation which is illustrated as below:

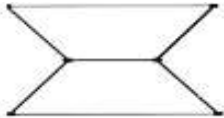


Figure 2.7.5– Hourglass mode

Obviously, the element distorts in such a way that the angle between diagonals alters and the length remains unchanged, and eventually the angles between the sides in the vertices keep out the original angles-90- defined for an optimized element.

The strains and underlying forces are computed based on the velocities and/or coordinates of diagonally opposite nodes of the quadrilateral elements; with this in mind and considering the probable situation mentioned in previous paragraph, one notice that the strain will not increase when the length of diagonals remains unchanged. When the hourglassing mode occurs, the energy does not alter and due to this fact, it is called zero energy mode.

To prevent this unphysical phenomenon, corrective forces are considered to resist the hourglass modes of deformation.

Below is the hourglass card applied for all parts including: bonnet outer skin, bonnet inner skin and torso impactor and etc.:

Table 2.7.1 – Hourglass parameters

<i>IHQ</i>	<i>QM=QB=QW</i>	<i>Q1</i>	<i>Q2</i>
4	0.03	1.5	0.06

2.7.5 Velocity

2.7.5.1 Initial velocity of rigid torso impactor

According to the torso impact test setup, the velocity of the impactor was defined as 6.1 [m/s] along the normal vector of contact surface's elements of the impactor via Inivel card and the velocity was applied to the entire nodes of the impactor using Set-Node feature of SetD card.

2.7.5.2 Initial velocity of headform impactors

And the velocities of the head-form impactors were defined as 11.1 [m/s] based on Euro NCAP standard and available test report, along the impact angles defined in the Euro NCAP standard as 65° for adult impactor and 50° for child impactor.

2.7.6 Impactor Positioning

2.7.6.1 Rigid Torso Impactor

As can be seen in the following figure, the positions of the torso impactor in two

experiments conducted at Autoliv Co. have been depicted. In the first experiment named L212009, the impactor was aligned from one side on the rear edge of the bonnet and in the meantime, on the centerline of the bonnet which was parallel to the vehicle's longitudinal axis. See figure 2.7.6.

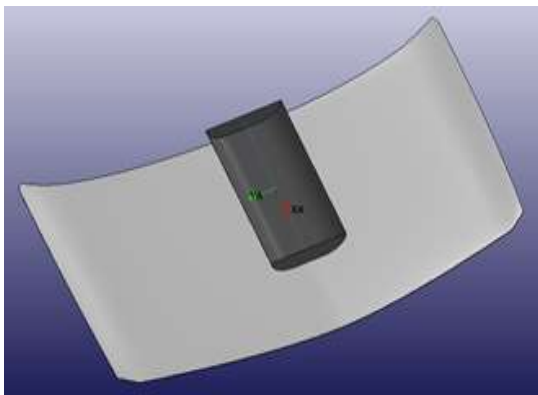


Figure 2.7.6– Rear-aligned impactor

In the second test, the impactor is manipulated to the front end of the bonnet, but not on the centerline, this time the impactor was located in an offset distance around 125 mm towards the right edge of the bonnet. See figure 2.7.7.

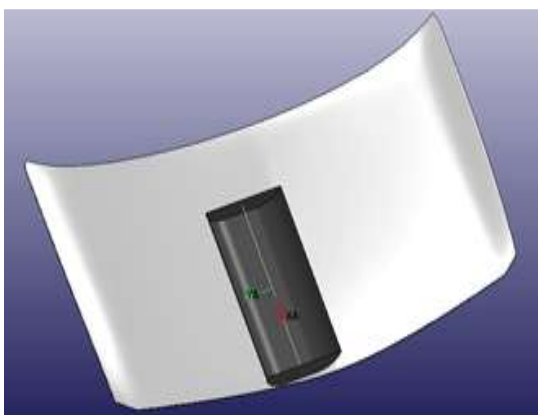


Figure 2.7.7– Front-aligned impactor

For both experiments, the impactor's contact surface is kept parallel to the bonnet impact surface.

2.7.6.2 Head-form Impactors

There were two different sources of the impact positions in the Euro NCAP report. First one was the coordinates of the impact positions depicted in the figure below, and second one was the photos captured after impacts which were available in the Euro NCAP report. It was detected from the coordinates table that there were some errors in the coordinates and it is evident from the figure 2.7.8 that the coordinates of the impact positions namely CP07, CP01 are far from the impact zone. Also, the comparison of the coordinates table and photos of the impacts revealed that the impacts positions specified as CP09 and CP08 are not in the right positions.

Therefore, using the combination of impacts photos and the coordinates table, the impactors were manipulated to the positions illustrated in the figure 2.7.9.

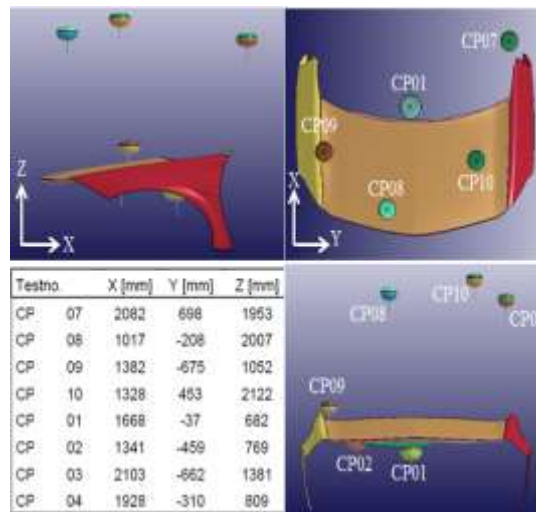


Figure 2.7.8– Positions of head-form impactors based on Euro NCAP test report, TNO test no.: CP024205-CP024306

The upper row in the figure 2.7.9 shows the positions of the impactors manipulated and estimated visually and using the wrong coordinates. In the lower row of the figure 2.7.9, the corresponding views of the impact positions in which the impactors were manipulated based on the coordinates table of the Euro NCAP report are depicted.

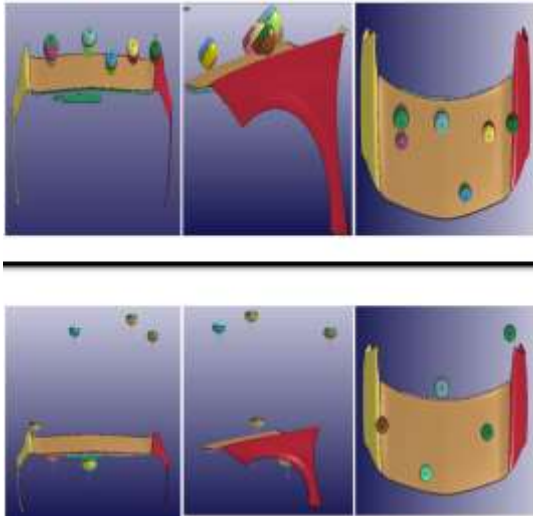


Figure 2.7.9– Positions of head-form impactors based on Euro NCAP test report, TNO test no.: CP024205-CP024306

The CP01 and CP02 were the positions where the adult head-form impactor collided to the bonnet; the CP07, CP08, CP09 and CP10 were the impact positions of the child impactor.

2.7.7 Accelerometer for Rigid torso impactor

Whereas the accelerometer has been mounted in the middle of the mechanical impactor, an accelerometer was modeled in the corresponding position at FE impactor; figure 2.7.10 illustrates the position and the relevant coordinate system including the direction of

the X, Y and Z-axes.

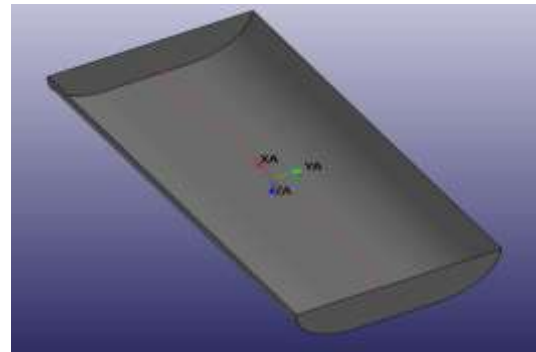


Figure 2.7.10– Position and coordinate system of the accelerometer

To define an accelerometer for the model, LS-DYNA needs 3 nodes to generate the position of the accelerometer by the first node, and the X-direction and Y-direction of the accelerometer's coordinate system between nodes 1, 2 and nodes 2, 3 respectively. To provide the first node for the accelerometer, a rigid beam has been constructed and connected to the rigid torso impactor at two points in the middle of the rear and front opposite sides of the impactor; the beam is split into two elements to create a node in the middle in which the origin of the accelerometer's coordinate system is placed. The motion of the torso impactor is followed by this rigid beam using `CONSTRAINED_RIGID_BODIES` card which merges the torso impactor and the rigid beam.

2.7.8 History node for rigid torso impact simulation

To obtain the displacement in the positions specified in the torso impact tests, two nodes were selected for each experiment in the

corresponding locations where the wire sensors have been connected to the bonnet's outer panel. Therefore, the displacement of those specific nodes were tracked and recorded during the simulations.

Figures 7.5.1 and 7.5.5 in appendix 7.5 show the positions of points where the wires were connected to the bonnet.

2.7.9 Miscellaneous

The units used for the Length, Mass, Time and Force were mm, Tone, second N respectively.

Gravitational force has been considered for whole the model using BODY_Z via LOAD tab and the magnitude of the acceleration equals to 9809.9980 mm/s² which was applied using CURVE via Define tab.

Time interval between outputs was set to 0.001s.

CONTACT_AUTOMATIC_SURFACE_TO_SURFACE card was used to provide the interface between different parts impacting one another. The coefficient of friction was set to 0.5; the magnitude of the acceleration is very sensitive to this coefficient, thus the aforementioned value was used as head-form impactor manual advised.

Inner skin and outer skin of the bonnet were connected to each other using spot weld at almost 70 % of total peripheral nodes of the bonnet.

Furthermore, the plates of the hinges and the U-shaped latch of the bonnet which were eliminated in previous sections, being replaced by a few constraints recognized as

SPC-Node in LS-DYNA. Since the aim of the preparation of the model in LS-DYNA is for kinematic research, thus the strength of these parts and the connection area are not given a prominent.

3 Results

3.1 Preliminary Control

3.2 Adult Head-Form Impactor CP01

3.3 Adult Head-Form Impactor CP02

3.4 Child Head-Form Impactor CP10

3.5 Child Head-Form Impactor CP09

3.6 Child Head-Form Impactor CP08

3.7 Child Head-Form Impactor CP07

3.8 Rigid Torso Impactor

3.1 Preliminary Control

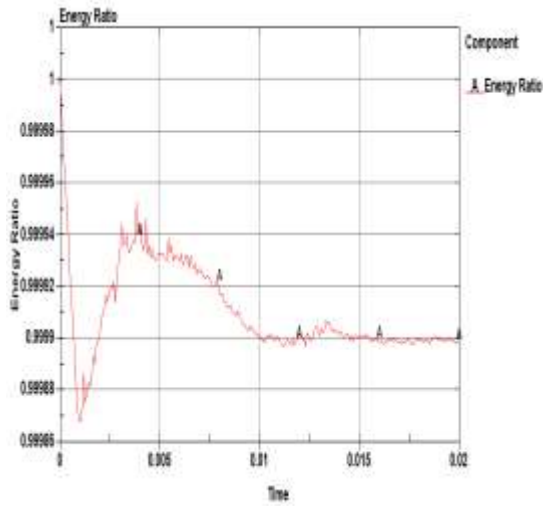


Figure 3.1.1 - Energy Ratio

As illustrated in the figure above, the energy ratio is almost 1, implying that the energy balance is approximately perfect; also, this is evident in the energy plot where the total energy is almost constant during the impact.

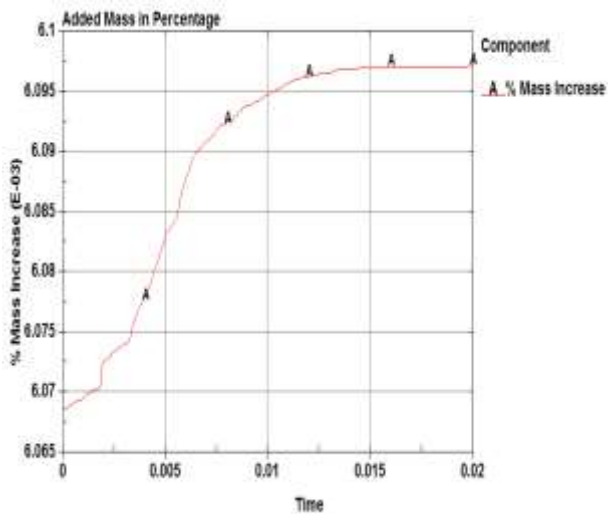


Figure 3.1.3- Added Mass

The added mass is around 0.006 % which is quite negligible and far from the limit which is advised (1% of physical mass). The hourglass energy is almost zero and these set of controls have been carried out for all the simulations

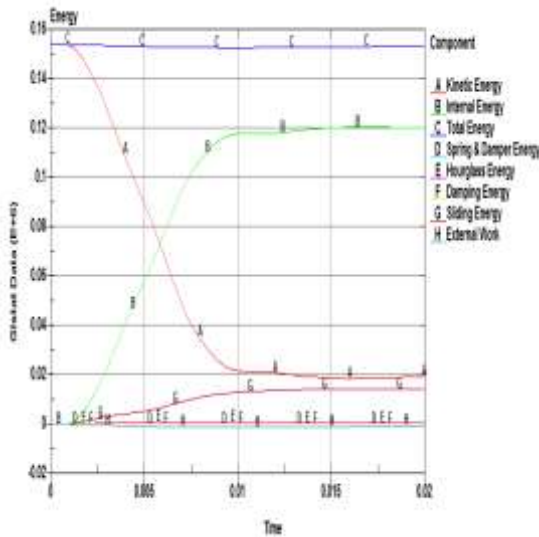


Figure 3.1.2- Energy Balance

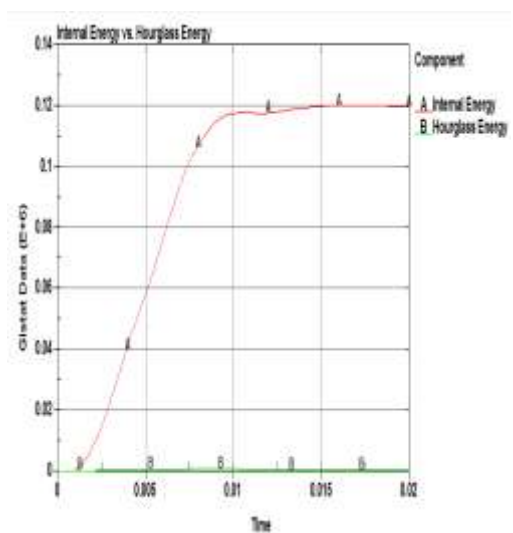


Figure 3.1.4- Internal Energy vs. Hourglass Energy

3.2 Adult HF Impactor CP01

3.2.1 Experiment vs. simulation

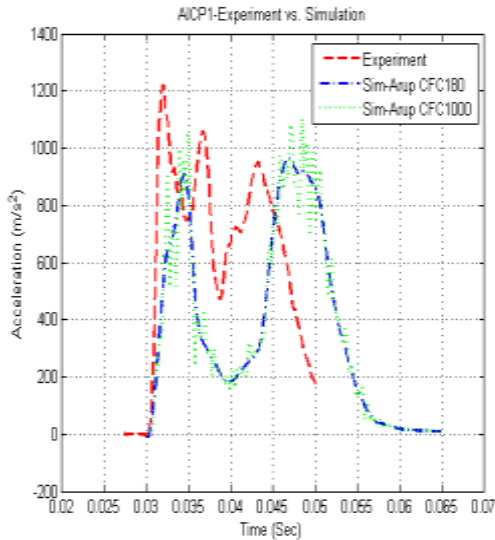


Figure 3.2.1- AICP1, Experiment vs. Simulation

The experiment, CP01, conducted at Euro NCAP lab was reconstructed in LS-DYNA at an approximately corresponding position. Figure 3.2.1 shows that the whole duration of the simulated impact is longer, occurring in 25 milliseconds, whilst the impact event is around 20 milliseconds in experiment. There are four extrema points in the experiment and among them, the peaks of acceleration curve are approximated well enough by simulation, but a discrepancy is observed at the minimum points of the simulation and the experiment in the region where the acceleration plunges between those two maximum points. In the simulation, the acceleration starts to increase after the first impact of the head-form impactor to the hood's outer skin, keeping on this upward trend a few milliseconds after impacting the outer skin to the inner skin; afterwards, the velocity decreases gradually and acceleration plunges to the minimum

point in which the third impact occurs between bonnet skins and engine cover and the acceleration surges to the second peak. Recall that all the components of engine housing have been defined as rigid parts in the simulations including engine cover (green) and frame (pink). It should be mentioned that the frame had been manipulated 200 mm downward in the simulated impact to avoid the collision of the bonnet and rigid frame (Figure 3.2.2); and this

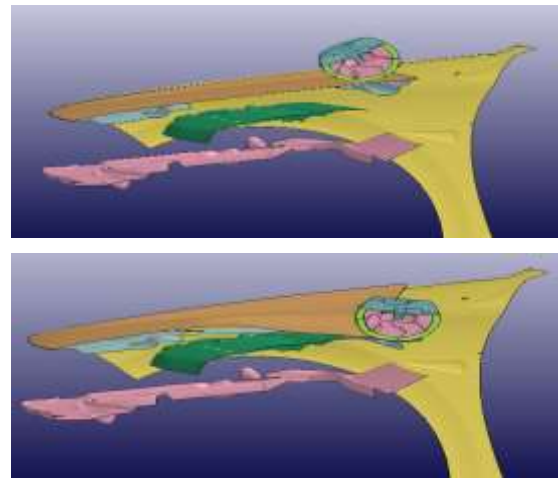


Figure 3.2.2, AICP1, Section view before and after impact

could be the cause of the difference between the minimum points of simulation and experiment. In presence of the rigid frame, the third impact point could have occurred earlier, and the magnitude of the minimum point in the simulation (20g) could be comparable with the corresponding point in the experiment (50g).

It should be noted that in visual inspection of the vehicle, the frame in its rear part was quite flexible and non-rigid unlike its front and side parts. And the effect of the presence of the frame was neutralized by downward translation due to the lack of data for its material and degrees of freedom.

3.2.2 Velocity comparison

An impactor velocity study was carried out at an approximately corresponding position specified in experiment no. CP01. The aim was to find out the effect of change in velocity varying within the tolerance limits of Euro NCAP testing standard, assuming that the velocity of impactor at the moment of the

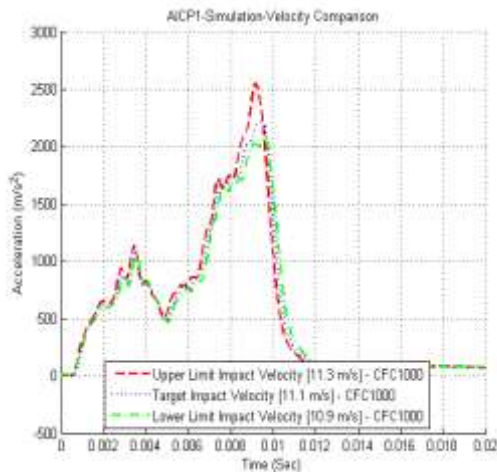


Figure 3.2.3- AICP1, Velocity Comparison

impact was within the tolerance limits.

The figure 3.2.3 shows how the peak of acceleration is altered when the velocity varies between 10.9 m/s and 11.3 m/s; obviously, the difference is significant and nearly 50g.

As can be seen in the figure 3.2.3, the minimum point (50g) of the acceleration curve is quite comparable with the corresponding point in the experiment result depicted in figure 3.2.1; and this is due to the position of the frame for this simulation. The rigid frame had not been translated downward in this simulation and it was in the original position so that the bonnet's panels collided

with the frame earlier than impact to the engine cover, causing the acceleration downturn at 50g. The peak is almost two times of the experiment's peak depicted in figure 3.2.1. The reason why the acceleration is higher than the first simulation or experiment, is due to the rigid material used for the frame in simulations; while the physical frame was plastic and flexible in its rear part. Despite considering one degree of freedom in Z direction for the frame, the large volume of this part along with its higher density (as the density of Steel) and the thicker shells considered for the contact stability caused the mass of the rigid frame to increase and subsequently, the resisting force (Inertia) increased; consequently, an acceleration with higher magnitude was generated in comparison with the first simulation or experiment illustrated in figure 3.2.1.

3.2.3 Impact angle comparison

The effect of impact angle was studied through the use of free motion headform impactor illustrated in figure 3.2.4. Two impact angles were simulated at an approximately corresponding position specified in experiment no. CP01. The impactor was made to hit the bonnet with

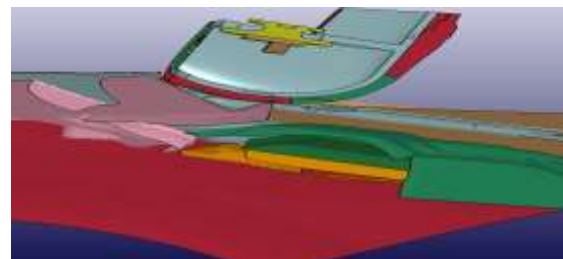


Figure 3.2.4- AICP1, Section view, Free Motion Impactor

forehead in one simulation, and in another simulation, the bonnet was hit with the face of impactor. The rigid frame (pink part in figure 3.2.4) fixed in space and was simulated as a zero-DOF part.

Figure 3.2.5 shows the comparison of the accelerations obtained in the aforementioned simulated impacts. The results show a

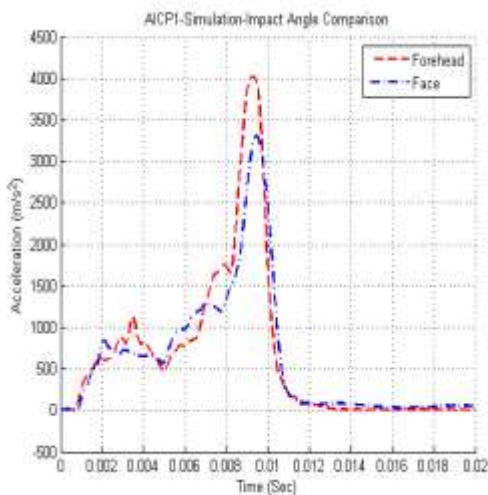


Figure 3.2.5-AICP1, Simulation, Impact Angle Comparison

discrepancy around 70g between two different impact angles, implying that the magnitude of the acceleration can be influenced significantly. On the other hand, the real impact angle should be monitored at the moment of the impact and the angle set in impactor launcher could be not enough and accurate.

In this set of simulations, even greater acceleration magnitude appears due to the little space between the bonnet and the frame and also the zero-DOF constraint defined for the rigid frame in the simulations.

3.3 Adult HF Impactor CP02

3.3.2 Different Materials

3.3.1 Experiment vs. simulation

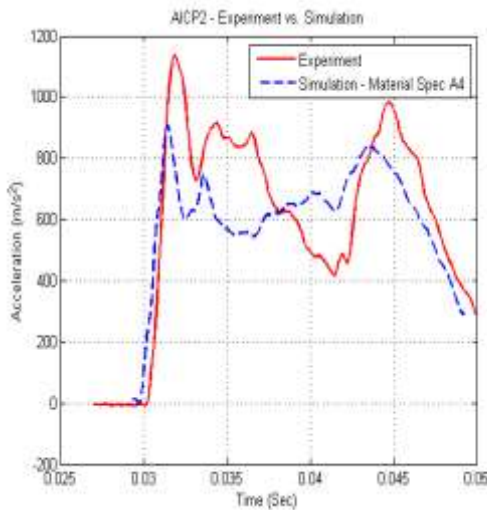


Figure 3.3.1-AICP2, Experiment vs. Simulation

The experiment no. CP02 was reconstructed using the FE model of the vehicle and the FE free motion headform impactor depicted in figure 3.2.4; the rigid frame was translated 200 mm downward due to the previous explanation in section 3.2.1.

It is apparent from the figure 3.3.1 that the duration of impact is almost identical in both experiment and simulation, implying that the FE model approximates the duration of impact well enough.

Also it is evident that the maximum acceleration of the experiment is nearly 20g higher than the simulation. But it should be noted that the FE model of free motion headform impactor is around 100gr lighter than the FE model of Euro NCAP headform impactor, generating less kinetic energy and less acceleration magnitude which could be a cause of slightly lower acceleration.

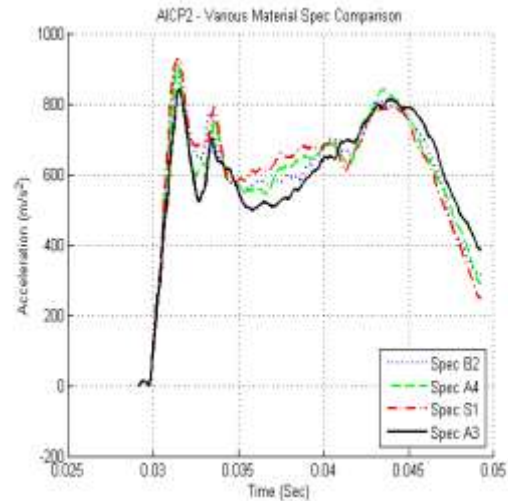


Figure 3.3.2- AICP2, Material Comparison

Using free motion head-form impactor and four different material specifications with similar mechanical properties, four simulations have been run in the second impact position where the experiment has been conducted. Figure 3.3.2 shows that the duration of the impact event in the simulation is almost equal to the duration of the impact event in the experiment; the acceleration magnitudes are comparable. It is clear that even similar materials having similar elasticity modulus, yield strength and ultimate strength show different behaviors which are obvious in the results.

3.4 Child HF Impactor CP10

3.4.1 Experiment vs. simulation

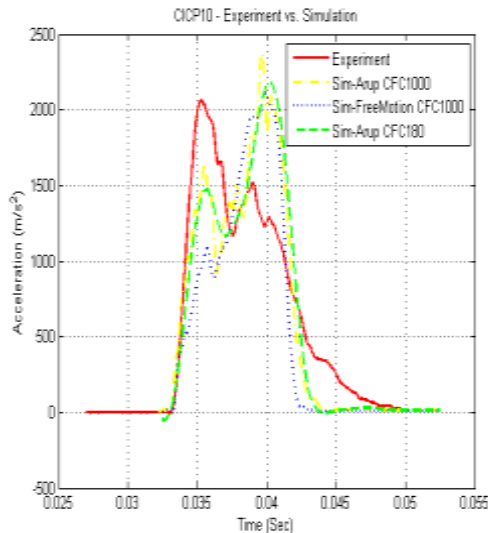


Figure 3.4.1- CICP10, Experiment vs. Simulation

The test no. CP10 was simulated using a Euro NCAP FE model of child headform impactor and the FE model of the vehicle front at an approximately corresponding position.

Obviously, the peak values and the impact durations of experiment data and simulation data are quite similar, showing that approximately identical areas are swept under both acceleration curves. At the first glance, one can notice that the first and the second peaks of the experiment and the simulation are mirrored; precisely looking at the animation of the impact, deformation, impacted regions and strain values of the shells at impact zone reveal two points.

Firstly, soon after impact the acceleration

increases up to the first peak, but around that point the plastic behavior of the bonnet emerges. And the strain exceeds 2 %. Recall the stress vs. strain curve depicted in the figure 2.7.1, after around 1.5 % strain, the mechanical properties of the material enters to the plasticity where the slope of the curve is at least less than one third of the slope of the curve in the elasticity region. So, while the event is occurring in the elastic region with a sharp slope, the material becomes stiff and stiffer while the strain increases. Contrasting to elastic region, when the strain exceeds the yield strain, the slope of the curve decreases and the material become weak and weaker in plastic region, meaning that the resisting force against the impact decreases by increase in strain, causing less change in velocity and lower acceleration.

Secondly, after that slight decline, the acceleration surges again due to another impact which occurs between the inner skin of the bonnet and the edge of the rigid frame

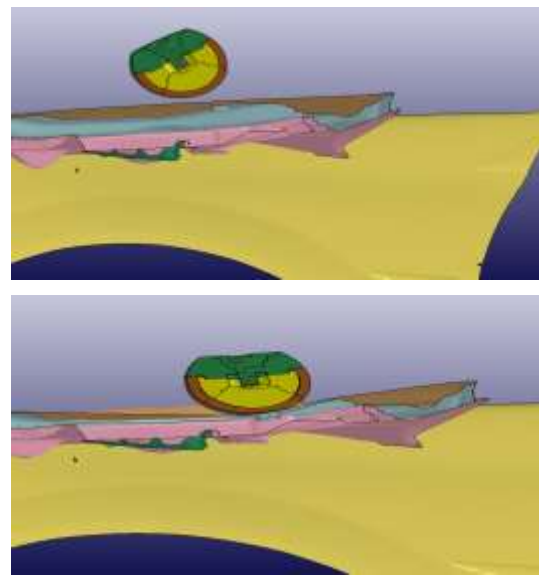


Figure 3.4.2- CICP10, Section view before and after impact

illustrated in figure 3.4.2. At this point, the deflection of the bonnet stops and the impactor start rotating around the contact point. And eventually, the acceleration decreases.

3.4.2 Thickness variation

Another simulation was carried out to investigate the effect of the thickness of the bonnet. Hence, the thickness of the inner skin and outer skin has simultaneously increased up to 0.05 mm for one case. And for the other case, the thickness of the panels has decreased up to 0.05 mm. It is observed from the results that the acceleration difference between the thinner and thicker panels is about 3 g over the entire domain. It seems that the change in thickness of the sheet metal within the tolerance limit does not make a big difference and is negligible. See figure 3.4.3.

Figure 3.4.4 shows the bonnet after impact and its deformation at the approximately corresponding position of the test no. CP10.

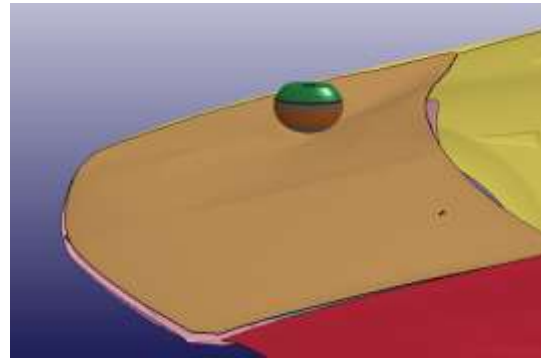


Figure 3.4.4- CICP10, Deformed Bonnet

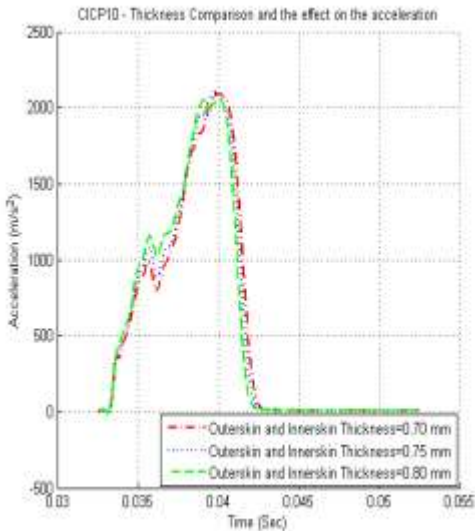


Figure 3.4.3- CICP10, Thickness Comparison

3.5 Child HF Impactor CP09

3.5.1 Experiment vs. simulation

The experiment no. CP09 was reconstructed in LS-DYNA at an approximately corresponding position. The results were found to be acceptable for the acceleration peak values, impact duration and the general shape of the curve. Figure 3.5.1

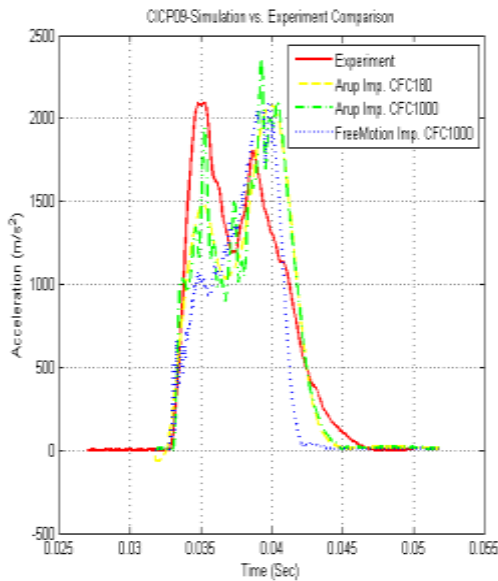


Figure 3.5.1- Experiment vs. Simulation

Also, two other studies have been carried out which are explained briefly as following:

3.5.2 Stiffness contribution

In the first study termed the levels of design, the contribution of different parts was investigated. The results imply that the rigid parts under bonnet have a significant contribution in impact and are hit by the bonnet during the impact event. The figure

3.5.2 illustrates when the impactor hits the bonnet including inner skin and outer skin, the acceleration magnitude does not exceed 150 g; the maximum magnitude of the acceleration is even lower around 100 g for the case in which the outer skin is only hit by impactor. But when the impactor hit the whole model including the bonnet inner and outer skins and the rigid parts under the bonnet namely: rigid frame and battery cover for this particular case, the acceleration reaches to the 150 g and 200 g at the first and second peak respectively. To approximate more reliable results, it is very important to manipulate the FE impactor model to the location where the mechanical impactor had hit the bonnet.

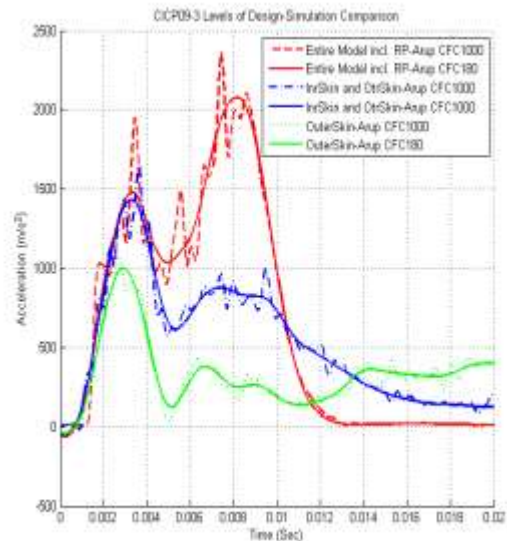


Figure 3.5.2- Stiffness Contribution Comparison

But the point is that either the impact position is measured after impact or before impact, there could be some uncertainty between the presumed target position and the real point of impact in the experiment. Therefore, the case

study depicted in the figure 3.5.3 was carried out to show the effect of positioning.

3.5.3 Positioning

Along with the main position, the free motion impactor has been moved up to 10 mm in the longitudinal direction for the second case and in the third case the impactor was moved 10 mm in the lateral direction. Figure 3.5.3 shows how the acceleration curve is influenced by deviation from the target position. The difference between the peak values of different simulation is nearly 15 g; however this is not a constant discrepancy over the entire domain. Moreover, the acceleration difference affected by the error in the impact position could be less or more, depending on the impact point (bonnet stiffness property), the layout of the components in the engine housing (gap/space between bonnet and components) and the stiffness of the aforementioned parts.

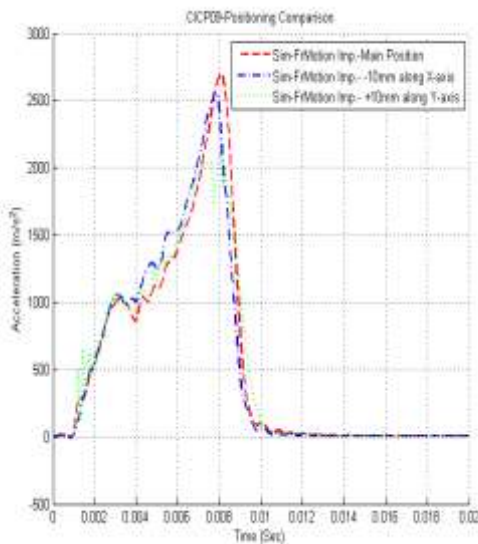


Figure 3.5.3- Positioning Comparison

And this is proven in the next set of simulation implemented in accordant with

test no. CP08.

Figure 3.5.4 shows how the bonnet is deformed after hitting by the impactor, implying that the side part of the rigid frame (pink part) is being collided with the bonnet.

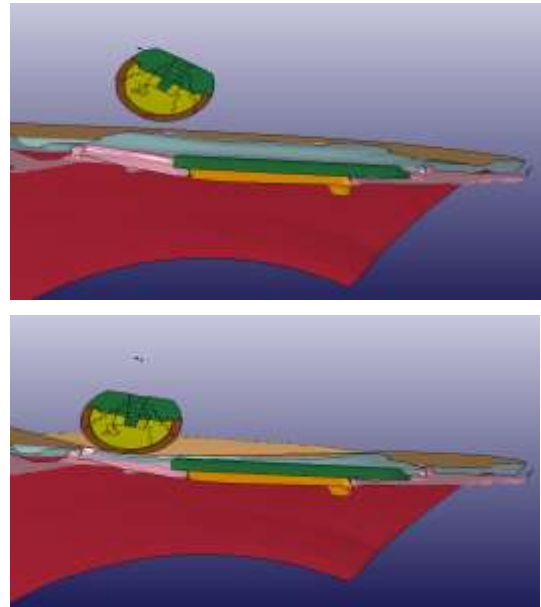


Figure 3.5.4- Section view, before and after impact

3.6 Child HF Impactor CP08

3.6.1 Experiment vs. simulation

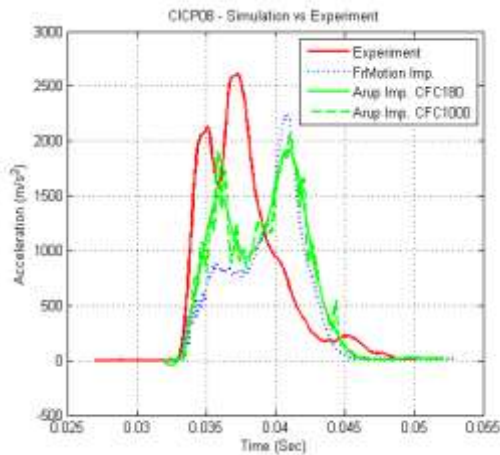


Figure 3.6.1- CICP08, Experiment vs. Simulation

The reconstruction of CP08 in FE model provided the acceleration of child headform impactor in comparison with the acceleration of mechanical impactor. See figure 3.6.1.

It is observed that the duration in simulated impact is 3 to 4 milliseconds longer than the duration of impact in the experiment; the maximum acceleration of simulated impact is 50g lower in the second peak.

Figure 3.6.3 shows that the impactor hit the bonnet at a point between the battery cover (green) and rigid frame (pink). Therefore, any change in the position of impact could alter the acceleration value and the duration of impact. It should be noted that the impact position was selected visually based on the

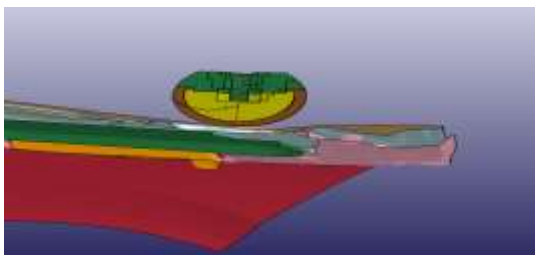


Figure 3.6.2- CICP08, Section view, before and after impact

photos of Euro NCAP tests which are available in appendix 7.4.1.

3.6.2 Positioning comparison

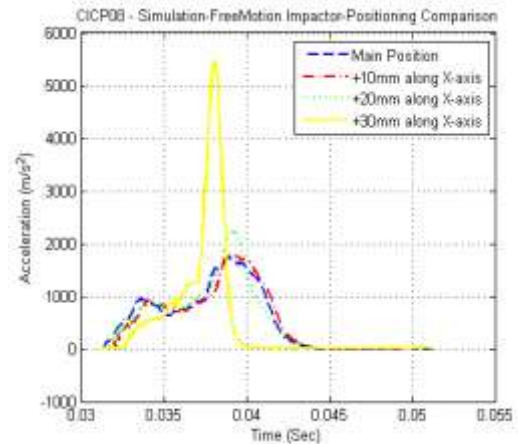


Figure 3.6.3- CICP08, Positioning Comparison

As can be seen, figure 3.6.2 illustrates the acceleration obtained through the simulation of impact in different positions with small deviations from the base impact position. This impact position was quite close to the edge of the rigid frame which was completely stiff, and fixed in its front part unlike its rear part which was flexible and non-rigid. The highest acceleration value among all four results belongs to the closest impact point to the rigid frame, implying that the role of the impact position is remarkable. The comparison of the acceleration shows the higher acceleration, the shorter duration of impact.



Figure 3.6.4- CICP08, Deformed bonnet

3.7 Child HF Impactor CP07

3.7.1 Experiment vs. simulation

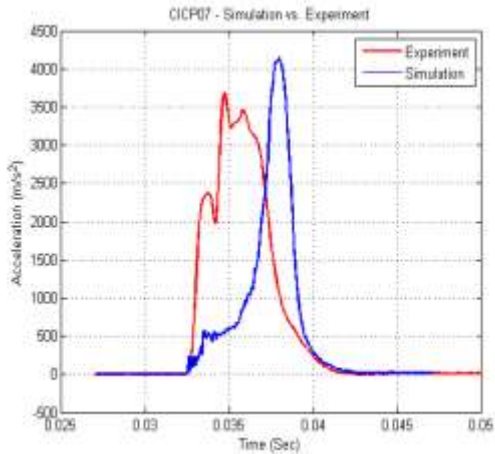


Figure 3.7.1– CICP07, Experiment vs. Simulation

At the position no.CP07, higher acceleration is observed due to the increased stiffness of impact zone. So the role of other contributing parts in impact like the left fender and the rigid part underneath the bonnet are identified. In the figure 3.7.1, the duration of impact is quite comparable, particularly when the acceleration starts to surge and also the end of impact when the acceleration reaches to zero, but it is a narrow band event in general compared to the experimental data. The peak value of the experiment is approximated well in the simulation.

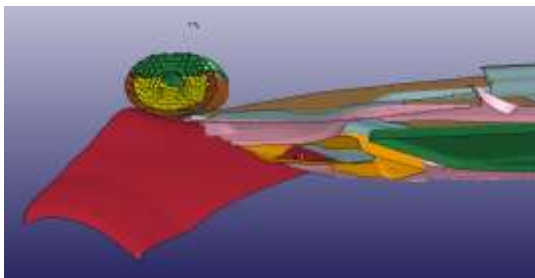


Figure 3.7.2– CICP07, Section view, after impact

3.7.2 Stiffness contribution

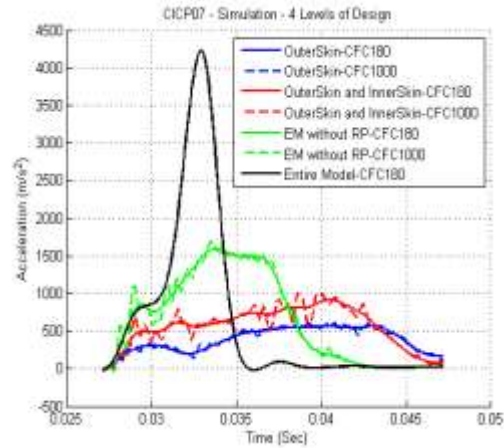


Figure 3.7.3– CICP07, 3 Levels of Design

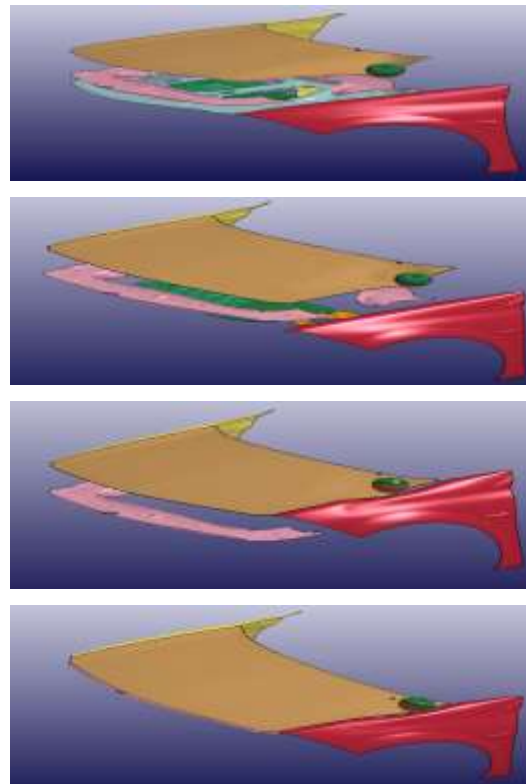


Figure 3.7.4– CICP07, Schematic of stiffness contribution of different part

3.8 Rigid Torso Impactor

3.8.1 Front edge alignment

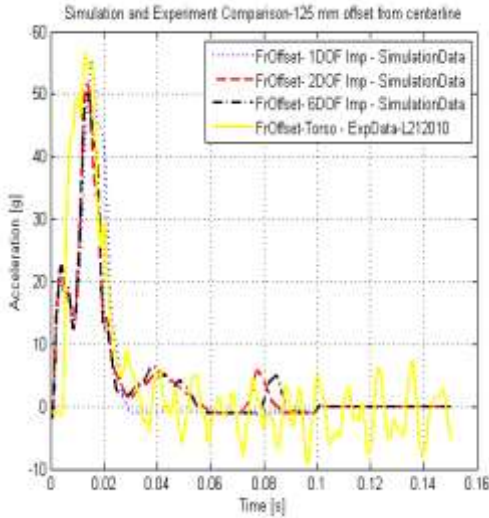


Figure 3.8.1– Torso Impactor, Front Edge Alignment, Acc

The acceleration and the duration of simulated impact are quite comparable with the experimental data. See figure 3.8.1.

3.8.2 Rear edge alignment

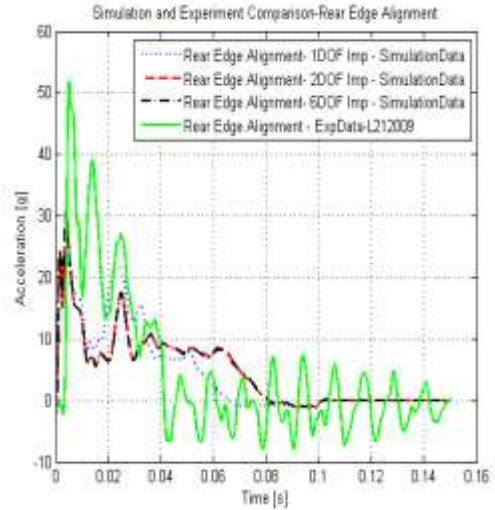


Figure 3.8.3- Torso Impactor, Rear Edge Alignment, Acc

The acceleration of the simulated impact in the second test conducted at the rear edge,

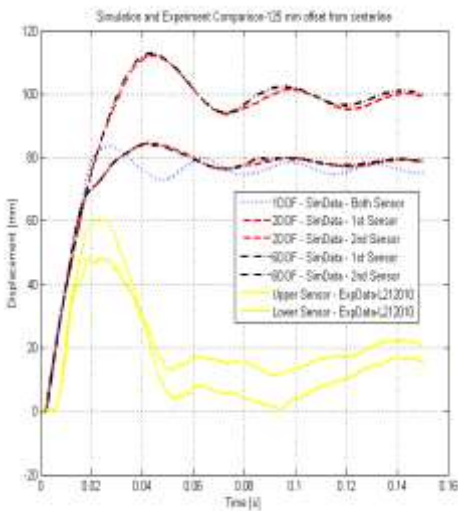


Figure 3.8.2– Torso Impactor, Front Edge Alignment, Disp

The displacement difference between experimental data and the simulated impact is around 20 mm, considering the impactor with one DOF. See figure 3.8.2.

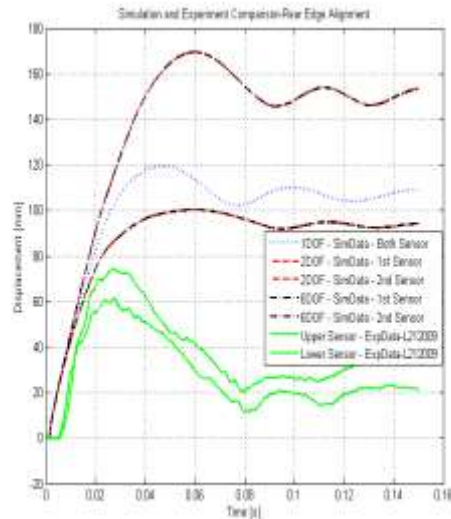


Figure 3.8.4– Torso Impactor, Rear Edge Alignment, Disp

figure 3.8.3, is lower than the experimental data. The acceleration in simulated impact reaches to almost 30g while the acceleration of mechanical impactor is around 50g. And

this does not make sense, because the impact region in rear part of the bonnet is weaker or less stiff compared to the front part where the rigid torso impactor hit the bonnet. The distance between the constraints at the rear part is significantly more than the distance between the constraints at the front part. Actually the distance between the constraints at the front is almost equal to the width of the rigid torso impactor, but the distance between the constraints in the rear part of the bonnet is almost equal to the width of the bonnet which is a significant difference. On the other hand, the regional mass of the bonnet in the rear edge alignment is less than the regional mass in the front edge alignment due to the blank space in the inner panel of the bonnet. Hence, the resisting inertia force in the rear part should be less than the front part. All of these reasons prove that the acceleration in the rear edge alignment should be less than front edge alignment. This is evident in the results of the simulated impacts, but the experimental data does not show this, implying that the results of the experiment in the rear edge alignment could be wrong.

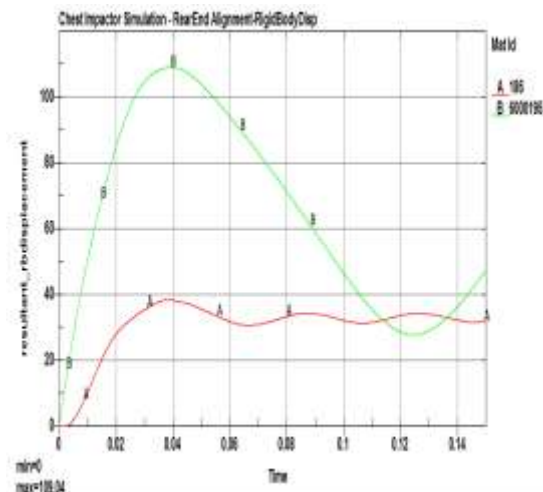


Figure 3.8.5- Torso Impactor, Rear Edge Alignment, Rigid Body Displacements of the Bonnet and the Impactor

Figure 3.8.5 illustrates the rigid body displacement of the bonnet and the rigid torso impactor in the simulated impact test. The approximate deformation of the bonnet can be obtained by subtraction of the rigid body displacement of the bonnet from the rigid body displacement of the rigid torso impactor.

Figure 3.8.6 shows the approximate deformation of the bonnet for the simulated impact test conducted at the rear part of the bonnet. The maximum deformation is comparable with the experimental data depicted in the figure 3.8.4.

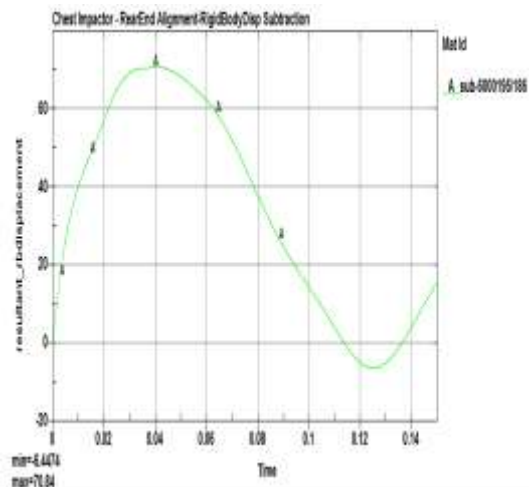


Figure 3.8.6– Torso Impactor, Rear Edge Alignment, Subtraction of the Rigid Body Displacements

Meanwhile, the simulation displacements depicted in the figures 3.8.2 and 3.8.4, are the nodal displacement recorded for the whole impact event via tracking two nodes.

4 Discussion

The results of the current study reveals that the complexity of the bonnet alter the impact acceleration significantly. In early stages of the thesis, the simplified, intermediate and advanced models were specified as inner skin, inner skin plus outer skin and inner skin plus outer skin including the effect of looseness of hinges and latch respectively. According to the results depicted in figure (44) and figure (53), the accelerations have increased 50% and 100% in those case studies. But on the other hand, the magnitude of the acceleration did not exceed 150 g for none of the impact positions. So, the structure of the bonnet by itself is able to absorb the energy of impact at the velocity defined in Euro NCAP standard, keeping the HIC value around the limit specified in pedestrian test protocol planned by Euro NCAP. This energy absorption capacity is due to the large deformation of the bonnet during impact. But what if the bonnet was forced to stop by another part? So this is the subtle point revealing the role of other contributing factors like the layouts of parts in engine housing, the gap between the bonnet and aforementioned components, the stiffness of the parts, their flexibilities and degrees of freedom. And all those high acceleration values obtained from simulations and experiments at different impact positions, prove that the energy absorption of the bonnet is reduced by the rigidity of the engine housing's components as well as the distance between the bonnet and the parts situated under the bonnet.

The acceleration of the impactors was the main criterion for the comparison and observation in all cases. The acceleration values are mostly affected by the stiffness of the engine housing's components and the gap

under bonnet. Impact velocity was another factor which was investigated; One tenth of one percent change in velocity showed a significant increase or decrease in peak acceleration up to nearly 10 %. The change in the thickness of the bonnet did not have a noticeable effect on the acceleration; and the acceleration difference was around 3g for the thickness variation of the sheet metal within the tolerance limit (0.1). However, the effect of the change in thickness beyond the aforementioned tolerance has not been investigated in this thesis; and the effect can be quite different, if one increase the thickness from 0.75 mm to 1.5 mm for instance. Also four different material specifications with very similar mechanical properties, were assigned to the bonnet and the results showed slight increase or decrease in peak acceleration compared to the peak acceleration of the main spec used in all case studies. Nonetheless, the acceleration fluctuations were noticeable over the entire duration of the impacts, implying that the heterogeneous material in a physical model can represent such behavior in practice; and their mechanical properties might vary from one point to another point. Finally, the study concerning the impact angle showed a remarkable change in acceleration for a large angle deviation from the value specified in standard.

As illustrated in the preliminary controls of simulation in previous section, the energy ratio is almost 1, implying that the energy balance is approximately perfect; and this is evident in the energy plot where the total energy is almost constant during the impact. The added mass is around 0.006 % which is quite negligible and far from the limit which is advised (1% of physical mass). The hourglass energy is almost zero and these set of controls have been carried out for all the simulations.

The results of the experiments and simulations exhibits that the peak of impact acceleration can be approximated with an acceptable degree of coherence; additionally, the impact duration was approximated well enough for the majority of cases.

But the discrepancy in the general shape of the acceleration curve was quite obvious between the experimental data and simulation data. Therefore the head injury criterion was utilized to interpret the differences due to the fact that the HIC value is sort of representing the swept area under the acceleration curve for a certain time interval.

The HIC values have been tabulated in the table (4.1) based on the available acceleration data of experiments and simulations and also the following formula:

$$HIC = \left\{ \left[\frac{1}{t_2 - t_1} \int_{t_1}^{t_2} a(t) dt \right]^{2.5} (t_2 - t_1) \right\}_{max} \quad (4.1)$$

As can be seen, the maximum value of the HIC has been extracted from the formula in two different methods of selecting the time interval; in the first one tabulated in the 3rd and 4th columns, the time interval was assumed 15 milliseconds and the maximum HIC value has been selected and tabulated for the entire domain of the impact duration. But in the second method tabulated in the 5th and 6th columns, the time interval varies between 1 millisecond and 15 milliseconds to find the maximum HIC value over the entire domain.

The HIC values of both methods show a plausible coherence between the experimental data and simulation data. Whilst the second method exhibit a better coherence with the peak acceleration, having a higher safety factor compared to the first method.

Table 4.1- HIC values comparison

	Exp. HIC15		Sim. HIC	Exp. HIC	Sim. HIC
	Rep. [6]	Acc. Data 15 ms	Acc. Data 15 ms	Acc. Data 1-15 ms	Acc. Data 1-15 ms
CP01	843	970	535	970	620
CP02	1093	793	590	792	590
CP07	1925	1489	1066	6337	5137
CP08	1154	1319	1083	3066	1909
CP09	5848	1169	1139	2249	2210
CP10	2190	1150	1192	2024	2308

So far, some of the causes of the difference between the experimental data and simulation data have been discussed using the results of the parametric studies carried out during the process of the investigation in this thesis. Aside from the fact that the FEM is an approximate solution and not an exact solution, and also the knowledge of the author of this report is not perfect, there could be other contributing factors influencing in the results of both experiments and simulations. So below are the major causes of the discrepancy between experiment and simulation given as a list:

- 1) Errors in the coordinates points of the impact positions in the experiments.
- 2) Lack of the material data and the degree of rigidity of the engine housing's components.

- 3) Lack of data regarding the degrees of freedom of the engine housing's components.
- 4) Difference in mechanical properties of the material spec assigned to the bonnet in the simulations and the material of the bonnets in the experiments.
- 5) Warpage of the bonnet during scanning due the difficulty in disassembling.
- 6) Scanning accuracy.
- 7) Lack of scan data in several zones of the bonnet due to the difficulty in disassembling.
- 8) CAD and Scan difference.
- 9) Mesh size and quality.
- 10) Accelerometer accuracy.
- 11) Initial velocity differences due to accuracy of the measuring tools.
- 12) Neglecting the effect of flexibility of the suspension mechanism.
- 13) Heterogeneous Material.
- 14) Euro NCAP Impactor uncertainty tolerance (20%).

5 Conclusion

The bonnet by itself can not represent the kinematics of the pedestrian in crash; and the stiffness effect of other parts and their positions should be considered in any simulation or experiment. Therefore in any design of vehicle front end in which the pedestrian safety is the purpose; enough space should be considered under the bonnet, allowing the bonnet get deformed to mitigate the effect of impact.

The results of this study work shows that the pop up bonnets can be popular among car manufacturers due to their capability in providing enough space for deflection during crashes, beside their role in launching an airbag mitigating the effect of the impact of the pedestrian in collision with the windshield.

Several contributing factors were introduced and investigated in this study work so that their effects can be a sort of guide in a design or a design development.

6 References

[1]. Dassault Systèmes (1999-2009): CATIA User's Documentation Home Page: http://catiadoc.free.fr/online/CATIA_P3_default.htm

[2]. EEVC (December 1998 with September 2002 updates): Working Group 17 Report Improved Test Methods to Evaluate Pedestrian Protection Afforded by Passenger Cars.

[3]. Euro NCAP (2012): Pedestrian testing protocol, URL: <http://www.euroncap.com/files/Euro-NCAP-Pedestrian-Protocol-v7.0--0-8a8d2050-444a-4d94-8556-35f6e058519.pdf>

[4]. Forsberg Ch. (2012): Renault Megane Hood tests report, Autoliv, Gothenburg, Sweden, 2012.

[5]. HyperWorks (2011) Desktop user's guide

[6]. J.P.L de Lang (2002): Pedestrian protection tests on a Renault Megane, *tests report no.: CP024205-CP024306*, Delft, Netherlands, 2002.

[7]. LS-DYNA (2006) Theory Manual 971, Livermore Software Technology Corporation.

[8]. Peng Y et al. (2012): Effect of pedestrian gait, vehicle-front geometry and impact velocity on kinematics of adult and child pedestrian head, *International Journal of Crashworthiness*, 17 (5) s. 553-561

[9]. Peng Y et al. (2011): Adult and child pedestrian head impact condition as a function of vehicle front end geometry, *International IRCOBI Conference on the Biomechanics of Impact*, September 14-16, 2011, Krakow, Poland, s. 255-264

[10]. Carter, E. L.; Neal-Sturgess, C. E.; Hardy, R. N. (2008): APROSYS in-depth database of serious pedestrian and cyclist impacts with vehicles, *International Journal of Crashworthiness*, Volume 13 (6): 629-642 Taylor & Francis – Dec 1, 2008

7 Appendices

7.1 Scan characteristics

7.2 CAD and scan comparison

7.3 Mesh

7.4 Head impact tests; Euro-NCAP

7.5 Rigid torso impact tests; Autoliv

7.1 Scans characteristics

Dimensions: 1061.691mm x 1426.96mm x 329.994mm (0.5m3)

Name: Front_Thin.1

=====
=====

Nb. cells = 1
Nb. points = 467360
Nb. visible points = 467360
Nb. activated points = 467360
Nb. filtered points = 0
Nb. triangles = 790222
Nb. boundaries = 831
Min extremity: -1640.567mm -942.085mm -0.605mm
Max extremity: 7.508mm 884.394mm 1026.311mm
Dimensions: 1648.075mm x 1826.478mm x 1026.916mm (3.091m3)

Name: Whole_Bonnet-Thin.1

=====
=====

Nb. cells = 1
Nb. points = 420799
Nb. visible points = 420799
Nb. activated points = 420799
Nb. filtered points = 0
Nb. triangles = 730605
Nb. boundaries = 760
Min extremity: -1245.714mm -810.024mm 732.196mm
Max extremity: -206.616mm 695.712mm 1066.216mm
Dimensions: 1039.098mm x 1505.736mm x 334.02mm (0.523m3)

Name: Engine-cutout_Thin.1

=====
=====

Nb. cells = 1
Nb. points = 1016162
Nb. visible points = 1016162
Nb. activated points = 1016162
Nb. filtered points = 0
Nb. triangles = 1472705
Nb. boundaries = 5304
Min extremity: -1258.224mm -720.623mm 648.989mm
Max extremity: -196.533mm 706.337mm 978.983mm

7.2 CAD and scan comparison

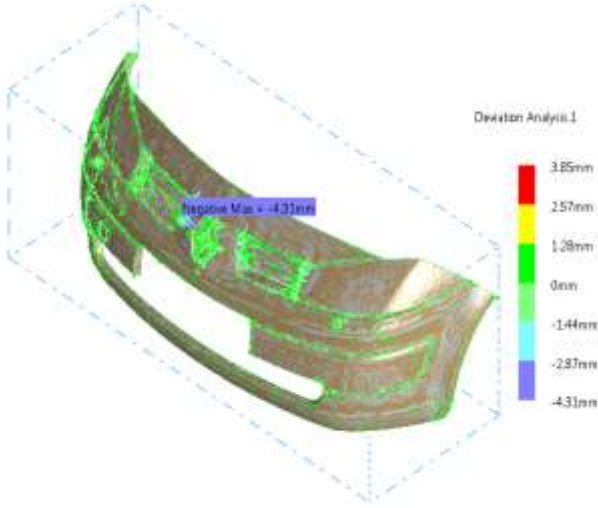


Figure 7.2.1- Bumper CAD Model

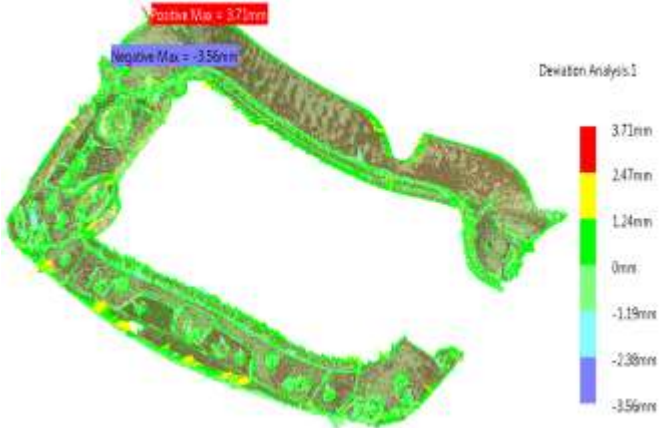


Figure 7.2.3- Frame CAD Model

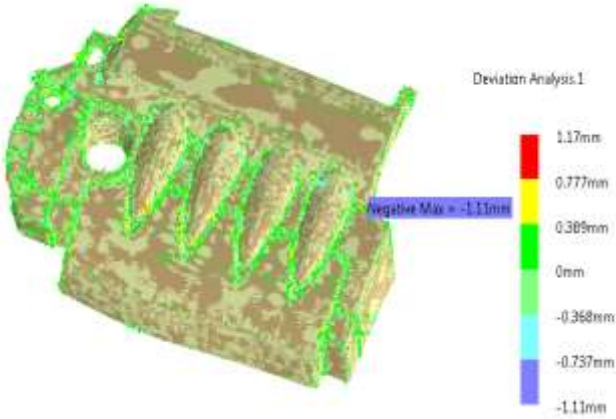


Figure 7.2.2- Engine Cover CAD Model

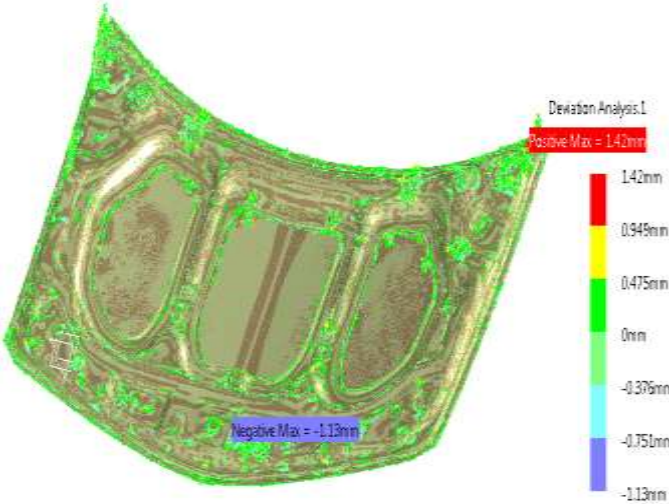


Figure 7.2.4- Bonnet CAD Model

7.3 Mesh

7.3.1 Meshed models

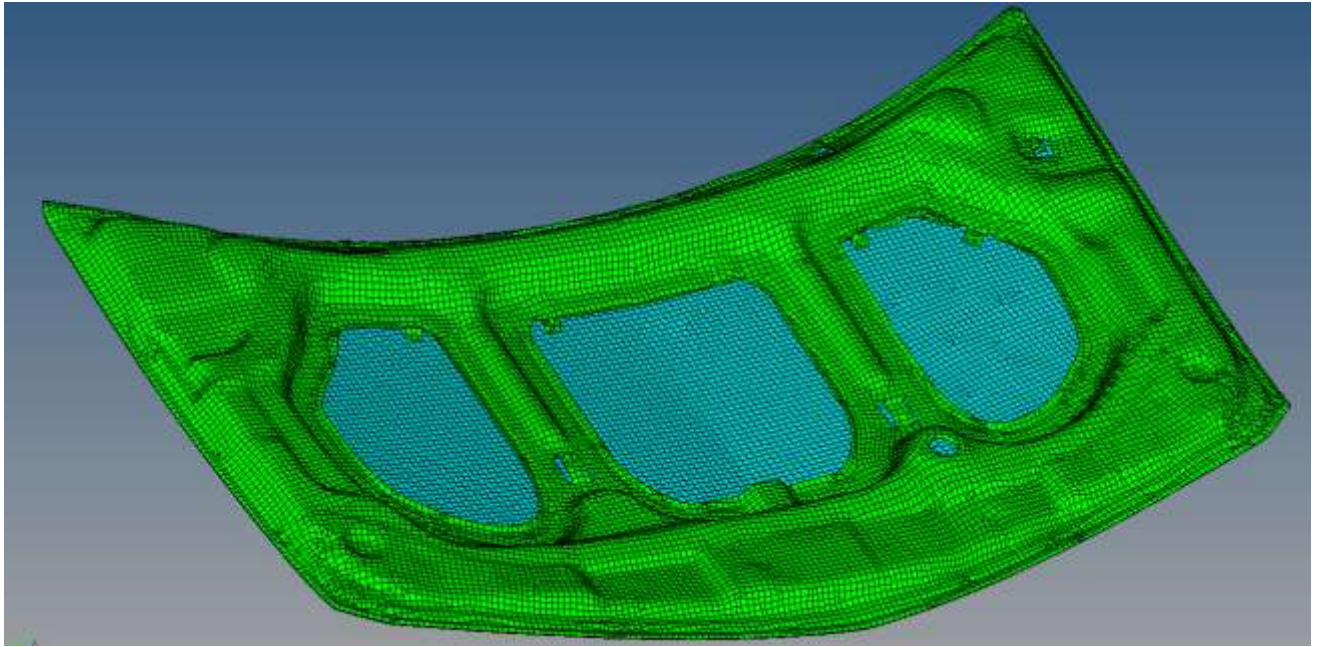


Figure 7.3.1- Meshed model of bonnet

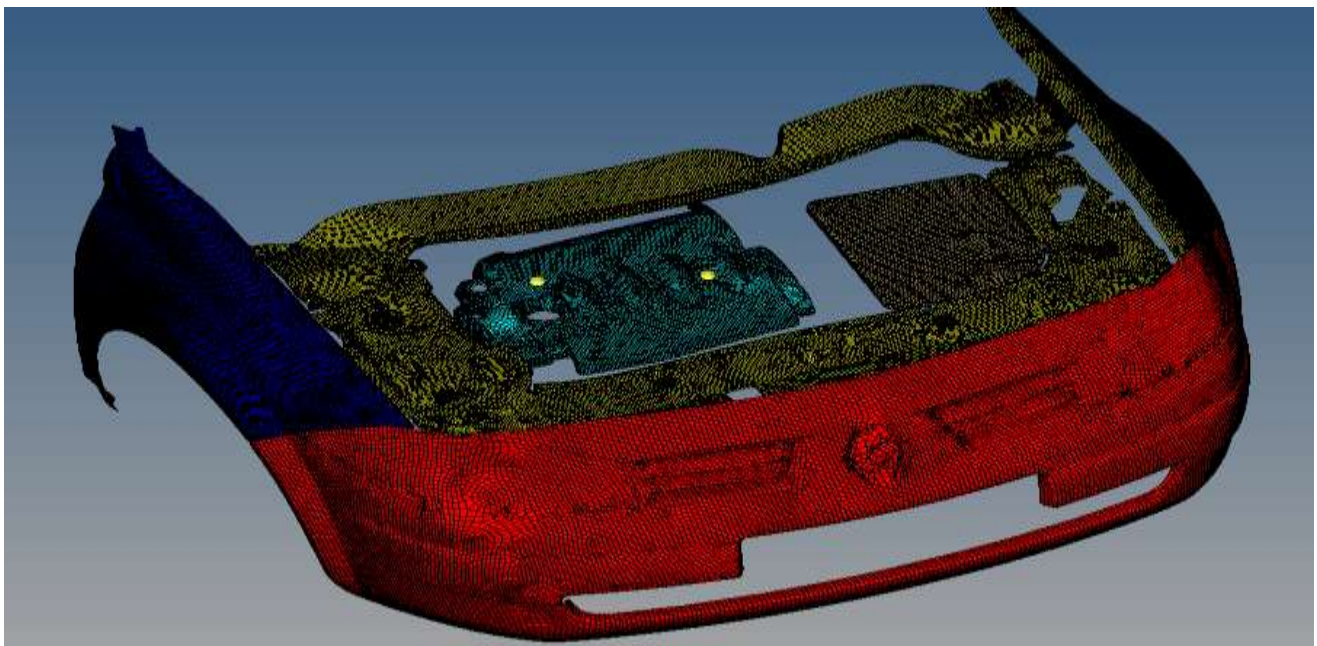


Figure 7.3.2-Meshed model of bumper, fenders, engine cover, battery cover and frame

7.3.2 Mesh quality report

2D Element Quality Report

This report was created by using the HyperMesh macro named '2D Elem QReport'.

Quality Check;	Limiting value;	# of Failed Elms;	% of Failed Elms
warpage >	15	0	0
aspect ratio >	5.0	1	0
skew angle >	60.0	1	0
length <	6	124588	100
jacobian <	0.6	0	0
min angle for quads <	40.0	0	0
max angle for quads >	136	12	0
min angle for trias <	15.0	1	0
max angle for trias <	140.0	1	0
% of trias	13		Result 6
# of duplicate elms			0
Total # of trias checked			7863
Total # of quads checked			116736
Total # of trias & quads checked			124599

NOTE:

The macro used to create this report does not evaluate master & slave elements. All other 2D elms, displayed on or off, are evaluated. HyperMesh's check elms panel evaluates displayed master & slave elms.

Figure 7.3.3- Mesh Quality Report

7.4 Head impact tests no. CP0242xx; Euro-NCAP

7.4.1 Visual inspection after tests



Figure 7.4.1- Impact position no. CP01



Figure 7.4.4- Impact position no. CP08



Figure 7.4.2 - Impact position no. CP02



Figure 7.4.5- Impact position no. CP09



Figure 7.4.3- Impact position no. CP07



Figure 7.4.6- Impact position no. CP10

7.4.2 Velocity, angle and mass

Table 7.4.1- Test Conditions [6]

Head Form Type	Impact Velocity [m/s]	Impact Angle	Mass [Kg]
Adult	11.1 ± 0.2	$65^\circ \pm 2^\circ$	4.8 ± 0.5
Child	11.1 ± 0.2	$50^\circ \pm 2^\circ$	2.5 ± 0.5

7.4.3 Impact position

Table 7.4.2- Impacts positions' coordinates [6]

Test no.	X [mm]	Y [mm]	Z [mm]	Impactor Type
CP01	1668	-37	682	Adult
CP02	1341	-459	769	Adult
CP07	2082	698	1953	Child
CP08	1017	-208	2007	Child
CP09	1382	-675	1052	Child
CP10	1328	453	2122	Child

According to the Euro NCAP report, *the reference for the coordinate in X direction is the 1500 mm forward of the center of the front wheels, the reference in Y direction is the longitudinal centerline of the vehicle and the reference in Z direction is ground level.* [6].

7.4.4 Head Injury Criterion

Table 7.4.3- HIC values [6]

Test no.	HIC15
CP01	843
CP02	1093
CP07	1925
CP08	1154
CP09	5848
CP10	2190

7.5 Rigid torso impact tests; Autoliv.

7.5.1 Test L212009

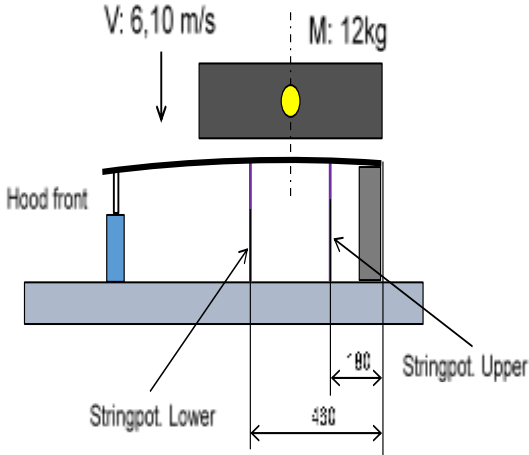


Figure 7.5.1- Wire sensor/Stringpot locations for rear edge alignment, provided by Christian Forsberg, Autoliv.



Figure 7.5.3- Constraints of rear part, provided by Christian Forsberg, Autoliv.



Figure 7.5.2- Constraints of front part, provided by Christian Forsberg, Autoliv.



Figure 7.5.4- Wire sensor/Stringpot for rear edge alignment, provided by Christian Forsberg, Autoliv.

7.5.2 Test L212010

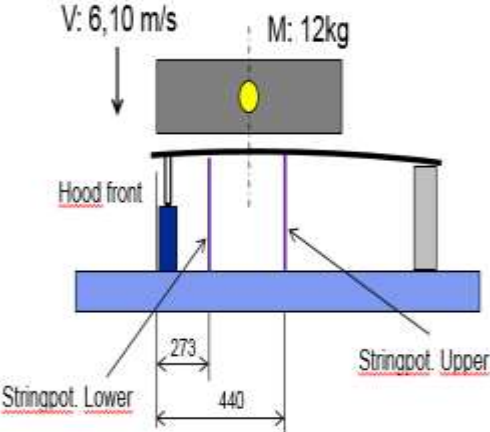


Figure 7.5.5- Wire sensor/Stringpot locations for front edge alignment, provided by Christian Forsberg, Autoliv.



Figure 7.5.7- Constraints of rear part, provided by Christian Forsberg, Autoliv.

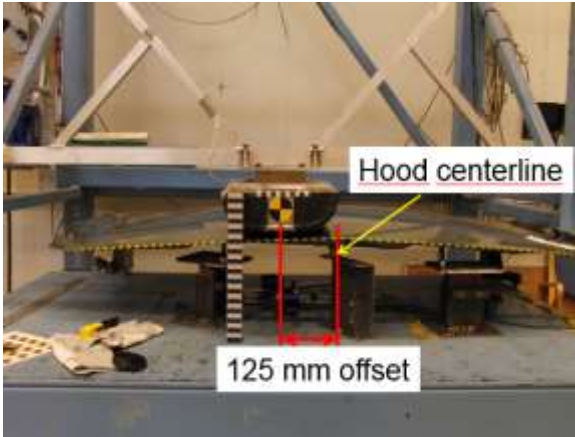


Figure 7.5.6- Rigid torso impact position, provided by Christian Forsberg, Autoliv



Figure 7.5.8- - Constraints of front part, provided by Christian Forsberg, Autoliv.